Fully localized and partially delocalized states in the tails of Erdös-Rényi graphs in the critical regime

M. Tarzia
LPTMC, CNRS-UMR 7600, Sorbonne Université, 4 Pl. Jussieu, F-75005 Paris, France
and Institut Universitaire de France, 1 rue Descartes, 75231 Paris Cedex 05, France

(Received 12 January 2022; revised 9 April 2022; accepted 25 April 2022; published 2 May 2022)

In this work, we study the spectral properties of the adjacency matrix of critical Erdös-Rényi (ER) graphs, i.e., when the average degree is of order $\ln N$. In a series of recent inspiring papers, Alt, Ducatez, and Knowles have rigorously shown that these systems exhibit a "semilocalized" phase in the tails of the spectrum where the eigenvectors are exponentially localized on a subextensive set of nodes with anomalously large degree. We propose two approximate analytical strategies to analyze this regime based respectively on the simple "rules of thumb" for localization and ergodicity and on an approximate treatment of the self-consistent cavity equation for the resolvent. Both approaches suggest the existence of two different regimes: a fully Anderson localized phase at the spectral edges, in which the eigenvectors are localized around a unique center, and an intermediate partially delocalized but nonergodic phase, where the eigenvectors spread over many resonant localization centers. In this phase, the exponential decay of the effective tunneling amplitudes between the localization centers is counterbalanced by the large number of nodes towards which tunneling can occur, and the system exhibits minibands in the local spectrum over which the Wigner-Dyson statistics establishes. We complement these results by a detailed numerical study of the finite-size scaling behavior of several observables that supports the theoretical predictions and allows us to determine the critical properties of the two transitions. Critical ER graphs provide a pictorial representation of the Hilbert space of a generic many-body Hamiltonian with short-range interactions. In particular, we argue that their phase diagram can be mapped onto the out-of-equilibrium phase diagram of the quantum random energy model.

DOI: 10.1103/PhysRevB.105.174201

I. INTRODUCTION

Since Anderson's celebrated discovery of localization more than sixty years ago [1], a huge amount of work has been devoted to the study of transport and spectral properties of quantum particles in random environments [2–4]. These investigations have deeply influenced the development of many areas of condensed matter physics, such as transport in disordered quantum systems, random matrices, and quantum chaos, just to name a few, and are still in the focus of current research, continuing to reveal new facets and subtleties.

In this context, the study of Anderson localization (AL) on sparse random graphs has attracted a strong and renewed interest in the last few years: On the one hand these treelike structures, which correspond to the infinite dimensional limit of the tight-binding model, allow in principle for an exact solution, making it possible to establish the transition point and the corresponding critical behavior [5–17]. On the other hand, the spectral properties of (weighted) adjacency matrices of sparse graphs encode the structural and topological features of many physical systems.

AL on sparse random graphs has been first studied by Abou Chacra, Anderson and Thouless [5], and then by many others [8–17]. Most of these works focused on the localization transition induced by the random potential. In a series of recent inspiring works [18–21], Alt, Ducatez, and Knowles studied instead the case in which localization is induced by the topology of the graph, and in particular by the strong fluctuations of the local connectivity. In particular, Alt *et al* studied the spectral properties of the adjacency matrix of Erdös-Rényi (ER) graphs in the critical regime (i.e., when the average degree is of order of the logarithm of the number of vertices) in absence of disorder in the local potential. In [18] the authors showed that the spectrum of these systems splits into (at least) two phases separated by a sharp transition transition: a fully GOE-like delocalized phase in the bulk of the spectrum, where the eigenvectors are completely delocalized [19], and a "semilocalized" phase near the edges of the spectrum, where the wave functions are exponentially localized on a subextensive number of vertices of anomalously large degree. In a subsequent paper [20], the same authors went a step further and proved the existence of a fully localized phase near the spectral edges.

These findings are particularly interesting at least for two reasons. First, ER graphs in the critical regime provide a natural representation of the topological features of the Hilbert space of generic interacting Hamiltonians with finite-range interactions [22]. Specifically, basis states of a many-body system chosen as eigenstates of the noninteracting part of the Hamiltonian (which can be straightforwardly diagonalized) correspond to vertices (or site orbitals) of the sparse graph, while interaction-induced couplings between them gives rise

to the links between the nodes. Take for concreteness a quantum spin-1/2 chain of n spins with nearest neighbor interactions. By choosing as a basis of the Hilbert space the simultaneous eigenstates of the operators $\hat{\sigma}_i^z$, the Hilbert space results in a n-dimensional hypercube of $N = 2^n$ sites (in absence of any symmetry on the global magnetization). Each configuration of n spins corresponds to a corner of the hypercube by considering $\{\sigma_i^z = \pm 1\}$ as the top/bottom face of the cube's nth dimension. The interacting part of the Hamiltonian, e.g., of the form of a transverse field $\Gamma \sum_i \hat{\sigma}_i^x$, acts as single spin flips on the configurations $\{\sigma_i^z\}$, and plays the role the hopping rates connecting "neighboring" sites in the configuration space. The quantum many-body dynamics can thereby be seen as single-particle diffusion on a very high-dimensional graph with a average degree equal to $n = \log_2 N$. Based on this analogy, for instance, it has been argued that AL on sparse random graphs offers a paradigmatic and intuitive representation of the so-called many body localization (MBL) transition [23]. In fact, during the last 15 years it was indeed established that quantum systems of interacting particles subject to sufficiently strong disorder will fail to come to thermal equilibrium when they are not coupled to an external bath even though prepared with extensive amounts of energy above their ground states [24–29]. To the extent that one of the most successful theories of physics, namely thermodynamics, is founded on the assumption of ergodicity, it is evident that whether or not many-body quantum systems constitute a heat bath for themselves, and hence are able to thermalize, is a very fundamental question. The analogy of this problem with single-particle AL was put forward in the seminal work of Ref. [22], where the decay of a hot quasiparticle in a quantum dot (at zero temperature) was mapped onto an appropriate noninteracting tight-binding model on a disordered treelike graph, and then further analyzed by later works in a more general context [22–24,30–33]. In this respect, a deep understanding of the spectral properties of critical ER graphs could give useful insight to make sense of more complex problems. In particular, below we will put forward a direct analogy between the phase diagram of critical ER graphs and the out-of-equilibrium phase diagram of the quantum random energy model (QREM), which is the simplest toy model featuring a many-body localized phase [34–38].

The second reason is that the appearance of states which are neither fully localized nor fully ergodic and occupy a subextensive part of the whole accessible volume has emerged as a fundamental property of many physical problems, including Anderson [39–41] and many-body localization [31,34–37,42–51], random matrix theory [52–68], Josephson junction chains [69], quantum information [38,70], and even quantum gravity [71]. Simple solvable dense random matrix models with independent and identically distributed (iid) entries, such as the paradigmatic Gaussian Rosenzweig-Porter (RP) model [52] and its generalizations [53–58] feature the appearance of fractal wave functions in an intermediate region of the phase diagram sandwiched between the fully ergodic and the fully localized phases. In these models, which have been intensively investigated over the past few years [72–79], every site of the reference space, represented by a matrix index, is connected to every other site with the transition amplitude distributed according to some probability law. In the latest years, other class of random matrix models featuring multifractal phases have emerged. These are one-dimensional systems with quasiperiodic potential in presence of a periodic drive [59–62] as well as in the static setting with p-wave superconducting order [63], and one-dimensional power-law random banded matrix models with strongly correlated translation-invariant long-range hopping [62,64–68]. In this context, ER graphs in the critical regime could provide yet another mechanism responsible for the appearance of partially delocalized but nonergodic states which complement the physical pictures provided by the families of models described above.

In this paper, we investigate the spectral properties of the adjacency matrix of critical ER graphs using both numerical methods and analytical arguments. The two main questions that we address are the following.

(i) What are the critical properties of the transition between the fully delocalized GOE-like phase in the bulk of the spectrum and the semilocalized phase near the spectral edges highlighted in Refs. [18,20]? How does the critical behavior compare to the one corresponding to standard AL on sparse matrices induced by the randomness of the local potential?

(ii) What are the spectral properties of such semilocalized phase? Is there a region of the phase diagram where eigenvectors localized around far away rare localization centers hybridize due to the exponentially small effective matrix elements between them?

In order to address these questions, we apply simple rules of thumb for localization and ergodicity and put forward an approximate treatment of the self-consistent cavity equations for the resolvent. These approaches provide a rough estimation of the phase diagram of the model. Our analysis suggests that the tails of the spectrum split in two phases separated by a mobility edge which separates fully localized eigenstates at the spectral edges (whose existence has been already rigorously proven in Ref. [20]), from an intermediate partially delocalized but nonergodic phase in which the wave functions hybridize (at least partially) around many resonating localization centers. In this region, the exponentially decaying tunneling amplitudes between localization centres are counterbalanced by an the large number of possible localization centers towards which tunneling can occur. We complement this analysis by extensive numerical calculations showing that the finite-size scaling behavior of several observables related to the statistics of the gaps and of the wave-function amplitudes is fully compatible with the theoretical results and allow one to determine the critical properties of the transitions.

The paper is organized as follows. In the next section, we define the adjacency matrix of ER graphs and provide a brief historical perspective on their study; In Sec. III, we review the recent exact results of Alt, Ducatez, and Knowles [18,20,21] on the semilocalized phase that emerges in the critical regime. In Sec. IV, we discuss the phase diagram of the model using two complementary analytical approaches. In Sec. V, we present several numerical results on the finite-size behavior of several observables related to the statistics of the energy gaps and of the wave-function amplitudes and discuss the critical properties of the transitions between the different phases. In Sec. VI, we characterize the statistics of the fluctuations of the largest eigenvalue of the spectrum. In Sec. VII, we

propose a mapping between critical ER graphs and the out-of-equilibrium phase diagram of the QREM. Finally, in Sec. VIII, we present some concluding remarks and perspectives for future investigations. In the Appendix, we present some supplementary information that complement the results discussed in the main text.

II. THE MODEL

The adjacency matrix of ER graphs is a real, symmetric $N \times N$ matrix $\mathcal{H}$ whose elements $\mathcal{H}_{ij}$ are (up to the symmetry $\mathcal{H}_{ij} = \mathcal{H}_{ji}$) iid random variables, with a Bernoulli probability distribution

$$p(\mathcal{H}_{ij}) = \left(1 - \frac{c}{N}\right)\delta(\mathcal{H}_{ij}) + \frac{c}{N}\delta\left(\mathcal{H}_{ij} - \frac{1}{\sqrt{c}}\right) \tag{1}$$

for $i \neq j$ and $\mathcal{H}_{ii} = 0$. (The off-diagonal elements are rescaled by $\sqrt{c}$ in order to have eigenvalues of order 1 for $N \gg 1$.) In the thermodynamic limit and for $c \ll N$, the degree of a given node, $k_i = \sqrt{c}\sum_j \mathcal{H}_{ij}$, is a random variable which follow a Poisson distribution $P(k) = e^{-c}c^k/k!$ of average $\langle k \rangle = c$ and variance $\langle k^2 \rangle - \langle k \rangle = c$.

The adjacency matrices of sparse random graphs encode the structural and topological features of many complex systems [80,81]. For instance, for random walks on graphs, the eigenvalue spectrum is directly connected to the relaxation time spectrum [82]. From the condensed matter perspective, the spectra of such matrices have been used for the characterization of many physical systems such as the study of gelation transition in polymers [83] and of the instantaneous normal modes in supercooled liquids [84].

ER graphs undergo a dramatic change in behavior at the critical scale $c \sim \ln N$, which is the scale at and below which the vertex degrees do not concentrate. For $c \gg \ln N$, all degrees are approximately equal and the graph is homogeneous. In this regime, ER graphs share the spectral properties of the GOE ensemble and the density of states (DoS) is given by the semicircle law (see also Ref. [85]). On the other hand, for $c \lesssim \ln N$, the degrees do not concentrate and the graph becomes highly inhomogeneous: it contains nodes of exceptionally large degree, leaves (i.e., nodes of degree 1), and isolated vertices (i.e., nodes of degree 0). ER graphs also have a percolation transition at $c = 1$. In fact for c strictly less than 1 with high probability (in the $N \to \infty$ limit) all connected components of the graph have size $O(\ln N)$, and there is no giant component. For $c > 1$, instead, there is with high probability a single giant component, with all other components having size $O(\ln N)$ [86,87].

Historically, the study of the spectrum of sparse symmetric ER adjacency matrices was pioneered by Bray and Rodgers in Ref. [88] (and in a similar context in Ref. [89] and later on in Ref. [90]) using the Edwards-Jones recipe. In their formulation, the evaluation of the average DoS $\rho(\lambda)$ relies on the replica method, which yield a very complicated integral equation. The same integral equation has been derived independently with a supersymmetric approach in Ref. [91] and later obtained in a rigorous manner in Ref. [92]. A variety of approximation schemes [93], such as the single defect approximation (SDA) [94] and the effective medium approximation (EMA) [95], were proposed to deal with the difficulty of solving the exact integral equation for the DoS. Almost in parallel, the cavity method [96] (see below) started to be employed for the determination of the spectral density of ER graphs [85,97]. A nice and comprehensive recent review of these studies can be found in Ref. [98].

In this paper, we focus on ER graphs in the critical regime, which, as discussed above, are particularly relevant as they represent a toy model for the Hilbert space of interacting Hamiltonian with finite-range interactions. Hence throughout the rest of the paper we will set $c = b \ln N$. Most of the numerical results presented below are obtained for $b = 0.5$.

III. THE SEMILOCALIZED PHASE

In their recent insightful work [18], Alt, Ducatez, and Knowles showed that the spectrum of ER graphs in the critical regime splits into (at least) two phases separated by a sharp transition at $\lambda = \lambda_{\rm GOE} = 2$: a GOE-like phase in the middle of the spectrum, $\lambda \in [-2, 2]$, where the eigenvectors are completely delocalized [19], and a "semilocalized" phase near the edges of the spectrum, $\lambda \in (-\lambda_{\max}, -2) \cup (2, \lambda_{\max})$, where the eigenvectors are essentially localized on a small number of vertices of anomalously large degree. In the semilocalized phase, the mass of an eigenvector is concentrated in a small number of disjoint balls centered around resonant vertices, in each of which it is a radial exponentially decaying function. [Throughout the following, we always exclude the largest eigenvalue of $\mathcal{H}$ associated to the flat eigenvector $1/\sqrt{N}(1, \ldots, 1)$, which is an outlier separated from the rest of the spectrum, see, e.g., Ref. [16] for more details].

Both phases are amenable to rigorous analysis. The semilocalized phase only exists when $b < b_\star = 1/(2\ln 2 - 1)$, while above $b_\star$ one retrieves the spectral properties of the homogeneous regime. For $b < b_\star$, the average DoS in the interval $\lambda \in (-\lambda_{\max}, -2) \cup (2, \lambda_{\max})$ is given asymptotically by $\rho^\infty(\lambda) \propto N^{\tau(\lambda)-1}$, where $\tau(\lambda)$ is an exponent whose explicit expression has been obtained rigorously in Ref. [18]. In particular, $\tau(\lambda)$ jumps discontinuously at the transition between the delocalized and the semilocalized phase from $\tau(\lambda) = 1$ for $\lambda \in [-2, 2]$ to $\tau = 1 - b/b_\star$ for $\lambda \to 2^+$ and $\lambda \to -2^-$.

The eigenvalues in the semilocalized phase were already analysed in Ref. [21] (see also Refs. [99–101]), where it was proved that they arise precisely from vertices of abnormally large degree [102]. More precisely, it was proved that each vertex with degree $k > 2c$ gives rise to two eigenvalues of $\mathcal{H}$ near $\pm\Lambda(k/c)$, where

$$\Lambda(x) = \frac{x}{\sqrt{x-1}}. \tag{2}$$

One can rigorously show that the number of those resonant vertices at energy $|\lambda| > 2$ is subextensive and asymptotically equal to the number of eigenvalues, i.e., $N\rho^{(\infty)}(\lambda) = N^{\tau(\lambda)}$. In other words, there is an approximate bijection between vertices of degree greater than $2c$ and eigenvalues larger than 2. Hence, in the limit of very large graphs, one than has that:

$$\rho^\infty(\Lambda(k/c))\left[\Lambda\left(\frac{k}{c}\right) - \Lambda\left(\frac{k-1}{c}\right)\right] \approx \frac{e^{-c}\,c^k}{2k!}.$$

After expanding for large k and changing variables $k \to \lambda$, one finds that

$$\rho^{\infty}(\lambda) \approx \frac{e^{-c}\, c^{1+c\tilde{\kappa}(\lambda)}}{2(c\tilde{\kappa}(\lambda))!}\tilde{\kappa}'(\lambda), \tag{3}$$

where

$$\tilde{\kappa}(\lambda) = \frac{\lambda}{2}(\lambda + \sqrt{\lambda^2 - 4}),$$
$$\tilde{\kappa}'(\lambda) = \frac{\mathrm{d}\tilde{\kappa}}{\mathrm{d}\lambda} = \frac{(\lambda + \sqrt{\lambda^2 - 4})^2}{2\sqrt{\lambda^2 - 4}}.$$

The function $\tilde{\kappa}(\lambda)$ above is the inverse of the function $\Lambda(x)$ given in Eq. (2), and gives the degree $c\tilde{\kappa}(\lambda)$ corresponding to an eigenvalue λ in the tails of the spectrum. The exponent $\tau(\lambda)$ is then simply defined as

$$\tau(\lambda) - 1 = \lim_{N\to\infty} \frac{\ln \rho^{\infty}(\lambda)}{\ln N}$$
$$= -b[\tilde{\kappa}(\lambda)\ln\tilde{\kappa}(\lambda) - \tilde{\kappa}(\lambda) + 1]. \tag{4}$$

The maximum eigenvalue $\lambda_{\max}(b)$ in the thermodynamic limit (which correspond to the largest degree of $\mathcal{H}$, see Ref. [20] and Sec. VI) is thus given by the value of λ at which $\tau(\lambda)$ vanishes,

$$\tilde{\kappa}(\lambda_{\max})[\ln\tilde{\kappa}(\lambda_{\max}) - 1] = \frac{1}{b} - 1, \tag{5}$$

and $b_\star$ is given by the condition $\lambda_{\max}(b_\star) = 2$.

In Ref. [18], Alt, Ducatez, and Knowles also investigated the structure of the eigenvectors and proved that in the semilocalized phase the wave functions associated to the eigenvalue at energy λ are highly concentrated around resonant vertices i such that $\Lambda(k_i/c)$ is close to λ, while the mass far away from the resonance vertices is an asymptotically vanishing proportion of the total mass. More precisely Alt *et al.* obtained an exact bound on the anomalous dimension D_∞ of the eigenvectors in the semilocalized regime. We recall that the anomalous dimensions are defined from the asymptotic behavior of the ℓ^{2q}-norm of the eigenvectors as

$$||\psi||_{2q}^2 = \left(\sum_i |\psi(i)|^{2q}\right)^{\frac{1}{q}} \propto N^{D_q(\frac{1}{q}-1)}$$

and fully characterize the geometric structure of the wave functions, allowing one to discriminate between ergodic, localized, and multifractal states. In the fully delocalized regime, $\psi(i) \sim N^{-1/2}$ uniformly on all the sites, and $D_q = 1$ for all q's. In the localized phase instead, the eigenstates are essentially concentrated in a small number $O(1)$ of vertices, and $D_q = 0$; In an intermediate multifractal phase, e.g, if the mass of ψ is uniformly distributed over some subset N^D of the sites, the D_q's take values between 0 and 1. Focusing on the $q \to \infty$ limit in the semilocalized regime in Ref. [18] it has been proven that the fractal dimension D_∞ is bounded by $\tau(\lambda)$ in the interval $D_\infty(\lambda) \in [0, \tau(\lambda)]$. This also implies that D_∞ exhibit a discontinuity in the thermodynamic limit as a function of the energies at $|\lambda| = \lambda_{\mathrm{GOE}} = 2$.

In a more recent paper [20], Alt, Ducatez, and Knowles went a step further and proved that the statistics of the eigenvalues near the spectral edges is described by the Poisson

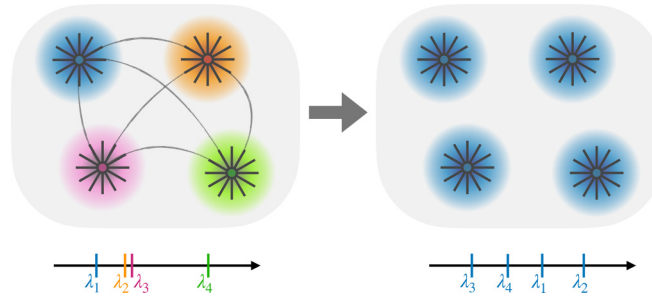

FIG. 1. Schematic illustration of the possible structure of the eigenvectors in the tails of the spectrum of critical ER graphs. Vertices of abnormally large degree $k = c\tilde{\kappa}(\lambda) > 2c$ play the role of localization centers. The wave functions decay exponentially around each vertex (shaded regions) and are connected by exponentially small effective tunneling amplitudes. Two situations are possible: these wave functions might hybridize (at least partially) around many resonant localization centers (right) or might stay fully localized around a single localization center (left). In the former case eigenstates close in energy occupy the same set of nodes and one has minibands in the local spectrum composed of $N^D \leqslant N\rho$ consecutive energy levels within which the Wigner-Dyson statistics is locally established due to level repulsion. In the latter situation instead, eigenfunctions nearby in energy do not overlap and the level statistics is of Poisson type.

statistics and the associated eigenvectors are exponentially localized around a *unique* center (i.e., $D_\infty = 0$). In other words they proved the existence of a fully localized phase in the edge of the spectrum of $\mathcal{H}$. However, this still leaves the possibility of the existence of an intermediate partially delocalized but nonergodic region sandwiched between the fully delocalized one and the fully localized one.

As a consequence of the analysis of Ref. [20], Alt, Ducatez, and Knowles also identify the asymptotic distribution of the largest (non trivial) eigenvalue of $\mathcal{H}$ [20], which is given by a law that does not match with any previously known universal distribution (see Sec. VI).

At this point, several key questions remain still open. Probably the two most important ones are the following.

(i) What is the nature of the semilocalized phase? Two scenarios are in principle possible. All eigenstates in the tails of the spectrum could be fully localized around a *unique* vertex (i.e., $D_\infty = 0$), or there could be a region of the phase diagram where eigenvectors are partially delocalized around *many* resonant vertices with the same degree (i.e., $0 < D_\infty < \tau$) due to the hybridization of the exponentially decaying part of the wave functions around each vertex, as schematically depicted in Fig. 1. In the first case, the level statistics should be of Poisson type, while in the second case it is reasonable to expect that level repulsion should arise among nearby energy levels which should form minibands in the local spectrum, giving rise to Wigner-Dyson statistics at least on the scale of the mean level spacing;

(ii) What are the critical properties of the transition(s) for the spectral statistics? What are the similarities and the differences compared to the standard localization transition observed in the Anderson tight-binding model on sparse graphs [5,8–17]?

In the following sections, we attempt to provide a tentative answer to these questions.

IV. THE PHASE DIAGRAM

As explained above, at an energy λ in the tails of the spectrum ($|\lambda| > 2$), we have $N\rho(\lambda)$ vertices of abnormally large degree $k = c\tilde{\kappa}(\lambda) > 2c$ that play the role of localization centers. The wave functions decay exponentially around each vertex. In this section, we attempt to determine whether it exists a region of the phase diagram where these wave functions hybridize (at least partially) due to the exponentially small tunneling amplitudes [103] between them (see Fig. 1 for a schematic illustration). In this case, wave functions close in energy occupy the same sets of nodes. Since the effective matrix elements between different localization centers and their energies are essentially uncorrelated, it is natural to expect that, in analogy with RP-type models with iid entries [52–54,56,73,74], the system forms minibands in the local spectrum composed of $N^D \leqslant N\rho$ consecutive energy levels within which the Wigner-Dyson statistics is locally established. Alternatively, all eigenstates in the tails of the spectrum can remain exponentially localized around a unique vertex. In this case, nearby eigenfunctions do not overlap and the level statistics is of Poisson type. Below we present two analytical arguments to address this question.

A. Rules of thumb criteria for localization and ergodicity

The first approach is based on the so-called "rules of thumb" criteria for localization and ergodicity which have been formulated in the context of dense random matrices with uncorrelated entries [53,54,56,74], and have been successfully adapted and applied in the latest years in the context of the MBL transition, where the subjacent adjacency matrix in the corresponding Hilbert space is sparse [34,37,48]. These "rules of thumb" essentially derive directly from first order perturbation theory for the eigenvectors and second order perturbation theory for the eigenvalues starting from the localized eigenstates. The basic idea is to posit the existence of exponentially localized wave functions around the localization centers of abnormally large degree, and to check whether these wave functions are perturbatively stable when the exponentially small matrix elements between them are turned on. Formally our approach consists in mapping the problem onto an effective RP model within each energy shell, and then in applying the rules of thumb to this effective model. To be more concrete, let us consider a given narrow energy shell around $|\lambda| > 2$ and let us consider the $N\rho(\lambda) \propto N^{\tau(\lambda)}$ exponentially localized wave functions centered around the localization nodes of degree $c\tilde{\kappa}(\lambda)$ with energies close to λ. These states constitute an effective RP random matrix model where $N\rho(\lambda)$ independent levels with average energy separation of order $\Delta = 1/(N\rho)$ are coupled by exponentially small off-diagonal transition rates due to the effective matrix elements between distant localization centers (see in particular Ref. [37] for a very similar mapping in the context of the QREM). Notice that the mapping onto an effective RP model here seems justified by the fact that the fluctuations of the energies of the localization centers of a given degree depend mostly on the fluctuations of the degrees of their neighbors [18,21] and are essentially uncorrelated from the effective tunneling amplitudes between them, which instead depend mostly on their distances (see below).

The first criterion, known as the Mott's criterion for localization, states that AL around a single localization center occurs when the level spacing $\Delta = 1/(N\rho)$ is much larger than the tunneling amplitude between localization centres. The second criterion [37,48,53,54,56,64,74], known as the Mott's criterion for ergodicity, is a sufficient condition for ergodicity. The idea is to estimate the average escape rate Γ of a particle sitting on a localization center using the Fermi Golden rule and compare it to the spread of energy levels. When the average spreading width Γ is much larger than the spread of energy levels, then the different localization centers are fully hybridized since starting from a given site the wave-packet spreads to any other localization center at the same energy in times of order one.

In order to apply these two criteria, we thus need to estimate the effective transition rates between two localization centers, which depend on their energy λ and on their distance r. This can be done at the level of the so-called forward-scattering approximation, which consists in retaining only the leading order of the perturbative expansion starting from the insulating phase [1,104]. This amounts in considering only the contribution to the nonlocal propagator at energy λ between two nodes of the graph at distance r coming from the shortest path connecting them, and ignoring loopy paths that contribute at higher order in perturbation theory. As discussed above, the nodes of abnormally large connectivity $k = c\tilde{\kappa}(\lambda)$ produce localized wave functions of energy $\lambda = \Lambda(k/c)$. Let us then consider two localization centers of abnormally large degree $k = c\tilde{\kappa}(\lambda)$ giving rise to two exponentially localized eigenvectors around them of energy close to λ. Let us suppose that these two nodes are at distance r on the graph, meaning that the shortest path connecting them is of length r (on a ER graph in the large N limit the shortest path connecting two nodes is with high probability unique). The question that one would like to answer is whether or not these two eigenvectors can be hybridized by the exponentially small matrix elements between them or not. In order to answer this question, we compute the nonlocal propagator at energy λ between these nodes at the leading order in the perturbative expansion in the hopping $1/\sqrt{c}$ as [1,104]

$$\mathcal{G}_r(\lambda) = \sum_{\text{paths } \mathcal{P}} \prod_{i \in \mathcal{P}} \frac{1/\sqrt{c}}{\lambda} \approx \left(\frac{1}{\sqrt{c}\lambda}\right)^r. \tag{6}$$

Since the $N\rho(\lambda) \propto N^{\tau(\lambda)}$ localization centers occupy random positions on the graph, the average distance between them is (asymptotically) given by the typical distance between two randomly chosen nodes, $r_{\text{typ}} = \ln N / \ln c$. (This can be also checked numerically, as shown in Fig. 13 of Appendix).

We then obtain that according to the Mott criterion, full localization around a unique vertex occurs when $|G_{r_{\text{typ}}(\lambda)}(\lambda)| < (N\rho(\lambda))^{-1}$, i.e.,

$$N^{[\tau(\lambda) - \frac{1}{2} - \frac{\ln \lambda}{\ln c}]} < 1.$$

In the thermodynamic limit (and in the critical regime, $c = b \ln N$), this condition is only fulfilled provided that

$\tau(\lambda) < 1/2$. (Note that the finite size corrections to the Mott's criterion decay very slowly, as $1/\ln\ln N$.) Using the asymptotic expression for the exponent τ given in Eq. (3), one then finally obtains an implicit equation for the mobility edge $\lambda_{\rm loc}$ which separates fully localized eigenstates, from an intermediate partially delocalized phase in which the wave functions hybridize (at least partially) around many resonating localization centers:

$$\tilde{\kappa}(\lambda_{\rm loc})[\ln\tilde{\kappa}(\lambda_{\rm loc}) - 1] = \frac{1}{2b} - 1. \tag{7}$$

Hence, for $|\lambda| \in (2, \lambda_{\rm loc})$, the exponentially decaying tunneling amplitudes between localization centres are counterbalanced by an the large number of possible localization centers towards which tunneling can occur and the eigenvectors are delocalized across many resonant localization centres. One should keep in mind however that Eq. (7) only provides a rough estimation of the mobility edge, since the analysis neglects the effect of the loops on the ER graphs as well as higher order terms in the perturbative expansion.

Since $\tau(\lambda)$ is a decreasing function of λ which tends to $1 - b/b_\star$ for $|\lambda| \to 2^+$, the existence of the intermediate nonergodic phase is only possible if $b < b_{\rm loc} = b_\star/2 = 1/(\ln 16 - 2)$. In Appendix, we will come back to this analysis suggesting a way to estimate an upper bound for the position of the mobility edge.

At this point, one can also wander whether in this intermediate partially delocalized phase the wave functions occupy all the $N^{\tau(\lambda)}$ localization centers at the corresponding energy or spread only over a subset N^{D_1} of them. In fact, the number of nodes on which the wave-function amplitudes are significantly larger than 0 is called the "support set" and its scaling with the system size is governed by the fractal exponent D_1 [105] [see Eqs. (17) and (18) below for a precise definition]. In the following, for simplicity and in analogy with the Gaussian RP ensemble, which provides the simplest example of an intermediate partially delocalized but nonergodic phase, we will make the (questionable) assumption that all the fractal dimensions are equal, i.e., $D_q = D$ for all q [52]. This amounts in supposing that the minibands in the local spectrum are locally compact (i.e., they are fractal but not multifractal). This is partially motivated by the plots of Fig. 5 below, which show that, although D_1, D_2, and D_∞ do not coincide quantitatively, they exhibit a very similar behavior.

In order to proceed further, we estimate the average escape rate of a particle sitting on a localization center and compare it to the spectral bandwidth at the same energy. Using the Fermi golden rule, the escape rate is approximately given by

$$\Gamma(\lambda) \approx 2\pi N\rho(\lambda)|\mathcal{G}_{r_{\rm typ}(\lambda)}(\lambda)|^2 \propto N^{[\tau(\lambda)-1-\frac{2\ln\lambda}{\ln c}]}. \tag{8}$$

This quantity corresponds to the average spreading of the energy levels due to the exponentially small hopping amplitudes between different localization centers. Assuming, as explained above, that minibands are locally compact as in the Gaussian RP model, this energy scale, usually called the Thouless energy $E_{\rm Th}$, coincides with the number of hybridized states within a miniband, N^D, times the mean level spacing, $(N\rho)^{-1}$. One than has [52,74]

$$\frac{1}{N\rho(\lambda)} N^{D(\lambda)} \propto \Gamma(\lambda).$$

Plugging the expression for $\Gamma(\lambda)$ given in Eq. (8) into the equation above, and using the fact that the average DoS behaves asymptotically as $N^{\tau(\lambda)-1}$ [18], one finds that in the thermodynamic limit the fractal dimensions are given by $D = 2\tau - 1$ (note that $D = 0$ at the localization threshold where $\tau(\lambda_{\rm loc}) = 1/2$):

$$D(\lambda) = \begin{cases} 2\tau(\lambda) - 1 & \text{for } 2 < |\lambda| < \lambda_{\rm loc}, \\ 0 & \text{for } |\lambda| > \lambda_{\rm loc}. \end{cases} \tag{9}$$

This function is plotted in Fig. 5 below for $b = 0.5$, and also pictorially illustrated in the left panel of Fig. 2. In Fig. 6 of Sec. V, we will provide a quantitative numerical test of the validity of this result.

The resulting phase diagram of the adjacency matrix of ER graphs in the critical regime obtained applying these simple arguments for localization and ergodicity is summarized in Fig. 2, showing the transition lines between the different phases. As discussed in Sec. VII, this phase diagram is, *mutatis mutandis*, qualitatively very similar to the one of the QREM recently obtained in Refs. [34–38].

B. Estimation of the localization transition from the cavity approach

A complementary approximate analytical strategy to tackle the localization transition and identify the position of the mobility edge as a function of the parameters of the model is based on the approximate treatment of the self-consistent cavity equations for the Green's functions.

In fact, the Green's function of the adjacency matrix of ER graphs satisfy an exact self-consistent equation in the thermodynamic limit [5,97]. The recursive equations are obtained by introducing the (cavity) Green's functions of auxiliary graphs, $G_{i\to j}(z) = [\mathcal{H}_{i\to j} - z\mathcal{I}]^{-1}_{ii}$, i.e., the ith diagonal element of the resolvent matrix of the modified Hamiltonian $\mathcal{H}_{i\to j}$ where one of the neighbors of i, say node j, has been removed. On an infinite tree, all neighbors $\{j_1, \ldots, j_{k_i}\}$ of a given vertex i with degree k_i are in different connected components of $\mathcal{H}$. By removing one of its neighbors j_a, one then obtains (by direct Gaussian integration or using the block matrix inversion formula) the following iteration relations for the diagonal elements of the cavity Green's functions on a given node i in absence of one if its neighbors as a function of the diagonal elements of the cavity Green's functions on the neighboring nodes in absence of i:

$$G^{-1}_{i\to j_a}(z) = -z - \frac{1}{c}\sum_{j_b\in\partial i/j_a} G_{j_b\to i}(z), \tag{10}$$

where j_a with $a = 1, \ldots, k_i$ denote the excluded neighbor of i, $z = \lambda + i\eta$, η is an infinitesimal imaginary regulator which smoothens out the polelike singularities in the right hand sides, and $\partial i/l$ denotes the set of all k_i neighbors of i except l. Note that for each site with k_i neighbors one can define k_i cavity Green's functions and k_i recursion relations of this kind, and hence on a finite ER graph of N nodes and average

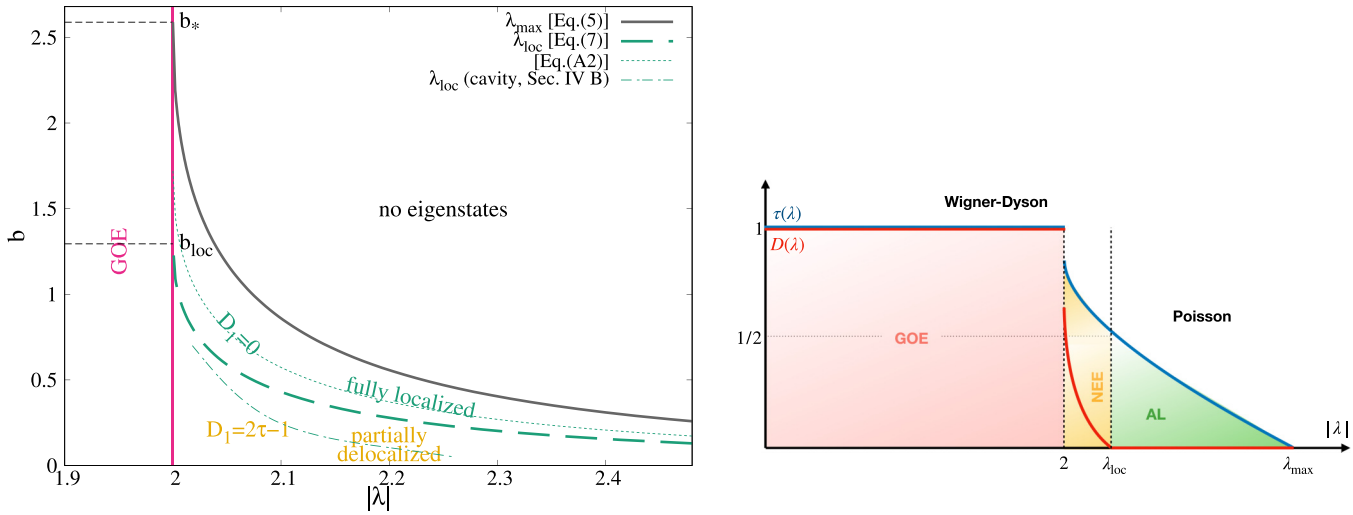

FIG. 2. (Left) Rough estimation of the phase diagram of the adjacency matrix of ER graphs in the critical regime, $c = b \ln N$, in the $(|\lambda|, b)$ plane obtained applying the Mott's criteria for localization and ergodicity. For $|\lambda| < 2$ in the bulk of the spectrum, the eigenvectors are fully delocalized and the DoS is given by the semicircle law. For $b < b_\star$ the spectrum is confined below the line $\lambda_{\max}$, given in Eq. (5). For $|\lambda| \in (\lambda_{\rm loc}, \lambda_{\max})$, the eigenvectors are fully localized around a unique localization center and the level statistics is of Poisson type [20]. For $|\lambda| \in (2, \lambda_{\rm loc})$, the wave functions partially delocalize around many resonant localization centers, due to the hybridization of energy levels. In this regime, the system exhibits minibands in the local spectrum and the Wigner-Dyson statistics is established locally up to the Thouless energy scale $E_{\rm Th} \equiv \Gamma \propto N^{D(\lambda)-\tau(\lambda)}$ much larger than the mean level spacing $\Delta \propto N^{-\tau(\lambda)}$, where $D(\lambda)$ is given by Eq. (9). The thick dashed line represents the estimation of the mobility edge obtained from the Mott's criterion, Eq. (7). The thinner dashed dotted line corresponds to the estimation of $\lambda_{\rm loc}$ obtained from the approximate treatment of the self-consistent cavity equations discussed in Sec. IV B. The dotted line shows the position of an upper bound for the mobility edge obtained in Appendix. (Right) Illustration of the behavior of the exponents τ and D as a function of the energy λ for fixed b in the interval $b \in (0, b_{\rm loc})$. In the fully delocalized GOE-like phase in the bulk of the spectrum, τ and D are identically equal to 1. In the tails of the spectrum, the exponent τ, which controls the asymptotic scaling behavior of the average DoS, is a decreasing function of λ exhibiting a finite jump from 1 to $1 - b/b_\star$ at $|\lambda| = 2$ and vanishing at $\pm\lambda_{\max}$ [see Eq. (4)]. According to the Mott criterion, AL around a unique localization center occurs when $\tau < 1/2$ (localization nodes are too rarefied to be hybridized), implying that $D = 0$ for $|\lambda| > \lambda_{\rm loc}$. Conversely, if $\tau > 1/2$ the eigenstates are partially delocalized around many resonant localization centers and the exponent D can be estimated from the Fermi Golden Rule, Eq. (9). At the transition in $|\lambda| = 2$, D is predicted to jump from 1 to $1 - 2b/b_\star$.

connectivity $\langle k \rangle = c$, Eq. (10) represents in fact a system of $\sim cN$ coupled equations.

After that the solution of Eqs. (10) has been found, one can finally obtain the diagonal elements of the resolvent matrix of the original problem on a given vertex i as a function of the cavity Green's functions for all the neighboring nodes in absence of i:

$$G_{ii}^{-1}(z) = -z - \frac{1}{c}\sum_{j_b \in \partial i} G_{j_b \to i}(z). \tag{11}$$

Although ER graphs are not loop-less infinite trees, in the large N limit, the neighborhood of i is, with high probability, a tree since the typical length of the loops grows as $\ln N/\ln c \propto \ln N/\ln\ln N$. One can then expect that if N is large enough Eqs. (10) and (11) provide a very good approximation of the true Green's functions (for $c > 1$ and finite it has been proven rigorously in Ref. [106] that the cavity equations becomes asymptotically exact in the thermodynamic limit).

The statistics of the diagonal elements of the resolvent encodes the spectral properties of $\mathcal{H}$. In particular, the local density of states (LDoS) is given by

$$\rho_i(\lambda) = \sum_{\alpha=1}^{N} |\psi_\alpha(i)|^2 \delta(\lambda - \lambda_\alpha) = \lim_{\eta \to 0^+} \frac{1}{\pi} {\rm Im} G_{ii}(\lambda).$$

From the LDoS, one can compute the average DoS, which is simply given by $\rho(\lambda) = (1/N)\sum_i \rho_i(\lambda) = 1/(N\pi){\rm Tr\,Im}G$. We will be also interested in the typical DoS, defined as $\rho_{\rm typ} = e^{\langle \ln {\rm Im}G \rangle}/\langle {\rm Im}G \rangle$.

Note that in principle the statistics of the LDoS allows one to distinguish between a localized and a delocalized phase. In fact, in a localized regime, the probability distribution of the LDoS is singular in the $\eta \to 0^+$ limit and characterized by power-law tails, while in a delocalized regime the LDoS is unstable with respect to the imaginary regulator η and its probability distribution converges to stable nonsingular η-independent distribution functions (provided that η is sufficiently small).

In the tails of the spectrum of the adjacency matrix of critical ER graphs, where $c \gg 1$ and the main contribution to the local DoS comes from the vertices of abnormally large degree $k > 2c$, it is very tempting to write an approximate equation for the Green's function in the spirit of the SDA [94,95], in which one uses the central limit theorem to evaluate the sums over the neighbors appearing in the right hand side of Eqs. (10) and (11). In fact, at least in the delocalized regime where the elements of the resolvent are described by a stable nonsingular distribution function in the $\eta \to 0^+$ limit, $(1/c)\sum_{j\in\partial i} G_{j\to i}(z)$ tends to a Gaussian random variable of mean proportional to k_i/c (which is of order 1) and variance proportional to $\sqrt{k_i}/c$ (which is of order $1/\sqrt{\ln N}$). Hence,

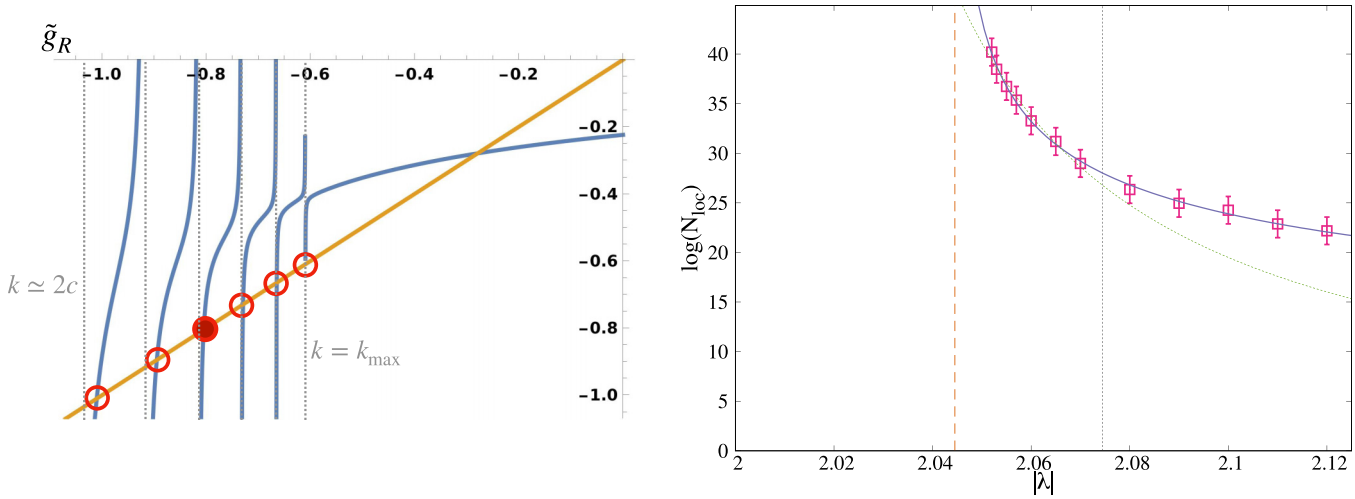

FIG. 3. (Left) Illustration of the procedure used to find the solution of Eq. (15). For each value of k between $2c$ and $k_{\max}$ the right-hand side of the equation has a pole at $\tilde{g}_R = -c\lambda/k$. Each one of these singularities produces a solution of the self-consistent equation (circles). We choose the solution associated to the value of the singularity in $-c\lambda/k_\star$, where $k_\star$ is the closest integer to $c\tilde{\kappa}(\lambda)$, which corresponds to the connectivity of the localization centers at energy λ in the thermodynamic limit. (Right) Logarithm of the smallest value of the system size for which Eq. (16) ceases to be satisfied, $N_{\rm loc}(\lambda)$ [107], as a function of the energy λ in the tails of the spectrum of critical ER graphs with $b = 0.5$. The continuous curve is a fit of the data of the form $\ln N_{\rm loc}(\lambda) \propto (\lambda - \lambda_{\rm loc})^{-\zeta}$, with $\lambda_{\rm loc} \approx 2.045$ and $\zeta \approx 0.258$. The estimation of the mobility edge obtained by this fit is represented by the dashed vertical line. The dotted vertical line shows the estimation of $\lambda_{\rm loc}$ obtained from the Mott criterion, $\lambda_{\rm loc} \approx 2.074$ (see also Fig. 2). Assuming that there is no intermediate phase and that $\lambda_{\rm loc} = 2$, one obtains a fit of the data represented by the green dotted curve, which corresponds to $\ln N_{\rm loc}(\lambda) \propto (\lambda - 2)^{-\zeta'}$ with $\zeta' \approx 1.08$.

neglecting completely the fluctuation of the local degrees, in the large N limit one can write an approximate equation for the average value of the Green's function restricted on the nodes of degree k, $\langle G\rangle_k = 1/(NP(k)) \sum_{i:k_i=k} G_{ii}$:

$$\langle G(z)\rangle_k \approx \frac{1}{-z - \frac{k}{c}\tilde{g}(z)}, \tag{12}$$

where $\tilde{g}(z)$ is defined as the average Green's function, $\tilde{g}(z) = \sum_k P(k)\langle G\rangle_k$. Summing over all degrees k with the corresponding probability $P(k)$, Eq. (12) finally leads to the following self-consistent equation for $\tilde{g}(z)$:

$$\tilde{g}(z) \approx -\sum_k \frac{P(k)}{z + \frac{k}{c}\tilde{g}(z)}. \tag{13}$$

Once the solution of the equation above is found, using Eq. (12), one can obtain an approximate expression for the whole probability distribution of the elements of the Green's function as

$$Q(G) \approx \sum_k P(k)\,\delta\left(G + \frac{1}{z + \frac{k}{c}\tilde{g}(z)}\right). \tag{14}$$

In the thermodynamic limit and for $|\lambda| \in (2, \lambda_{\max})$ one expects that the sum over k is dominated by the nodes of connectivity $k = c\tilde{\kappa}(\lambda)$. In Figs. 8–11, we discuss the quality of this approximation with respect to the exact solution of the cavity equations for several observables and for several values of λ and N (and for $b = 0.5$).

At this point, in order to determine the position of the mobility edge, one can seek for solutions of Eq. (12) in absence of the imaginary part of $\tilde{g}$, and then study the stability of these solutions with respect to the addition of a small imaginary part. The approximate self-consistent equation for the real part of $\tilde{g}$ is

$$\tilde{g}_R = -\sum_k \frac{P(k)}{\lambda + \frac{k}{c}\tilde{g}_R}, \tag{15}$$

where the sum over k is in fact cut-off at $k_{\max}$ which is the largest degree on a graph of N nodes. The right-hand side of the equation above has poles at all values of $\tilde{g}_R$ such that $\tilde{g}_R = -c\lambda/k$. For λ and N fixed, each pole is associated to a particular value of the degree between $k = 2c$ and $k_{\max}$. As illustrated in the left panel of Fig. 3, each one of these singularities produces a crossing between the right-hand and the left-hand sides of the equation and gives rise to a solution of (15). We assume that in the thermodynamic limit the relevant solution is the one associated to the value of the singularity in $-c\lambda/k_\star$, where $k_\star$ is the closest integer to $c\tilde{\kappa}(\lambda)$, which corresponds to the connectivity of the localization centers at energy λ. This assumption is partially justified by the plots of Fig. 9 below, showing that the average DoS restricted to the nodes of connectivity k indeed peaks around $k_\star$ as N is increased.

Adding now a small imaginary part to the average Green's function and linearizing with respect to it, one obtains the self-consistent equation describing the exponential decay or the exponential growth of the imaginary part starting from the real solution. The stability condition of the localized phase is thus simply given by

$$\frac{1}{c}\sum_k \frac{kP(k)}{\left(\lambda + \frac{k}{c}\tilde{g}_R\right)^2} < 1. \tag{16}$$

We have solved numerically Eqs. (15) and (16) for several values of b, varying the energy λ and the system size N [and choosing the solution of Eq. (15) which is the closest to the

pole in $-c\lambda/k_\star$]. This can be done for $N \lesssim 2^{50}$, since for N too large the exponentially small probability in the numerator and the poles in the denominator cannot be handled with a sufficient degree of numerical precision to yield reliable results. For every value of λ at fixed b, we determine the value of $N_{\rm loc}(\lambda)$, which corresponds to the smallest value of N such that Eq. (16) is satisfied [107]. The results of this procedure are illustrated in Fig. 3 for $b = 0.5$. One observes that $N_{\rm loc}(\lambda)$ increases very rapidly when λ is decreased and seems to diverge for $\lambda \approx 2.045$. This analysis suggests that in the thermodynamic limit and for $b = 0.5$ the mobility edge is located around $\lambda_{\rm loc} \approx 2.045$, which is in fact not too far from the estimation of $\lambda_{\rm loc}$ obtained from the Mott's criterion [Eq. (7) of Sec. IV A] for the same value of b, $\lambda_{\rm loc} \approx 2.074$. A similar behavior is found for other values of b. The estimation of $\lambda_{\rm loc}$ obtained from this analysis is plotted as a dashed dotted line in the $(|\lambda|, b)$ plane on the phase diagram of Fig. 2. Although the prediction for the mobility edge obtained from the approximate treatment of the self-consistent cavity equations does not coincide quantitatively with the one obtained from the Mott's criterion, the two lines have a similar qualitative shape.

For completeness, it is worth to mention that one can also try to fit the values of $N_{\rm loc}$ assuming that there is no intermediate phase and that the mobility edge is at $\lambda_{\rm loc} = 2$. However the quality of the fit (green dashed line) seems to be less good and limited to a narrower range compared with the fit obtained for $\lambda_{\rm loc} = 2.045$.

We conclude this section by noting that, similarly to the Mott criterion, within this approach delocalization occurs due to a trade-off between the exponential decrease of $P(k)$ and the accumulation of singularities in the denominator of Eq. (16) which become closer and closer to each other and make the sums over k blow.

V. NUMERICS

In this section, we present a numerical verification of the theoretical predictions for the phase diagram discussed above. We set $b = 0.5$ throughout. According to the phase diagram of Fig. 2, at $b = 0.5$ one should cross two phase transitions as the energy is increased. (1) A transition at $\lambda_{\rm GOE} = 2$ from the fully delocalized GOE-like phase to the partially delocalized but nonergodic phase, where the statistics of the wave-function amplitudes should exhibit a dramatic change (in particular the fractal dimension should display a discontinuous jump at the transition). (2) A AL transition at $\lambda_{\rm loc}$ where the gap statistics likely undergoes a transition from Wigner-Dyson statistics to Poisson statistics. In fact, as shown in Ref. [20], in the fully localized part of the spectrum above $\lambda_{\rm loc}$, the exponentially decaying eigenvectors around unique localization centers do not interact and the statistics of level spacing is Poisson. Conversely, as explained above, below $\lambda_{\rm loc}$ eigenstates close in energy are partially deolcalized around many resonant localization centers and, in analogy with RP-type models with iid entries, the system is expected to exhibit minibands in the local spectrum, within which the Wigner-Dyson statistics is established up to an energy scale much larger than the mean level spacing [52–54,56,73,74,76].

We employ two complementary numerical strategies to investigate these two transitions. The first approach consists in performing exact diagonalizations of the adjacency matrix of critical ER graphs of size $N = 2^n$ with n ranging from 9 to 18. Since we are interested in the properties of the tails of the spectrum, we only focus on a subextensive set of eigenvalues and eigenvectors in the spectral edges, $2 < |\lambda| < \lambda_{\rm max}$. The number of these eigenstates scales approximately as $\sim N^{1-b/b_\star}$ and the Lanczos algorithm works efficiently up to moderately large sizes. Averages are performed over (at least) 2^{43-2n} different independent realizations of the graph and over eigenstates in the same energy window.

The second strategy consists instead in solving directly the self-consistent cavity equations (10) and (11) on random instances of critical ER graphs of large but finite sizes $N = 2^n$, from $n = 12$ to $n = 28$. In practice, we first generate the graph according to the Bernoulli distribution (1). Then we find the fixed point of Eqs. (10), which represent a system of $\sim cN$ coupled equation for the cavity Green's functions. Finally, using Eqs. (11) we obtain the diagonal elements of the resolvent matrix on each vertex. We repeat this procedure 2^{32-n} times to average over different realizations of the graph. The advantage of this method over EDs is that the solution of the cavity equations can be obtained with arbitrary precision by iteration in a time that scales as $cN \propto N \ln N$, which is much faster than the computational time needed to diagonalize the Hamiltonian, which scales roughly as $N^{3-b/b_\star}$, thereby allowing one to access system sizes about 10^3 times larger.

A. Level statistics

Here we start by focusing on the AL transition. To this aim we perform a finite-size scaling analysis of the behavior of two observables related to the level statistics of neighboring eigenvalues. The first is the average ratio of adjacent gaps:

$$r_n = \min\left\{\frac{\lambda_{n+2} - \lambda_{n+1}}{\lambda_{n+1} - \lambda_n}, \frac{\lambda_{n+1} - \lambda_n}{\lambda_{n+2} - \lambda_{n+1}}\right\},$$

whose probability distribution displays a universal form depending on the level statistics, with $\langle r \rangle$ equal to 0.53 in the GOE ensemble and to 0.39 for Poisson statistics [108].

The second observable which captures the transition from Wigner-Dyson to Poisson statistics is given by the mutual overlap between two subsequent eigenvectors, defined as

$$q_n = \sum_{i=1}^{N} |\psi_n(i)||\psi_{n+1}(i)|,$$

In the Wigner-Dyson phase, $\langle q \rangle$ converges to $2/\pi$ (as expected for random vector on a N-dimensional sphere), while in the localized phase, two successive eigenvector are typically peaked around different sites and do not overlap and $\langle q \rangle \to 0$ for $N \to \infty$. At first sight, this quantity seems to be related to the statistics of wave functions' coefficients rather than to energy gaps. Nonetheless, in all the random matrix models that have been considered in the literature so far, one empirically finds that $\langle q \rangle$ is directly associated to the statistics of gaps between neighboring energy levels [56,109–111].

In the left panels of Fig. 4, we plot $\langle r \rangle$ (top) and $\langle q \rangle$ (bottom) as a function of λ for $b = 0.5$, showing that both

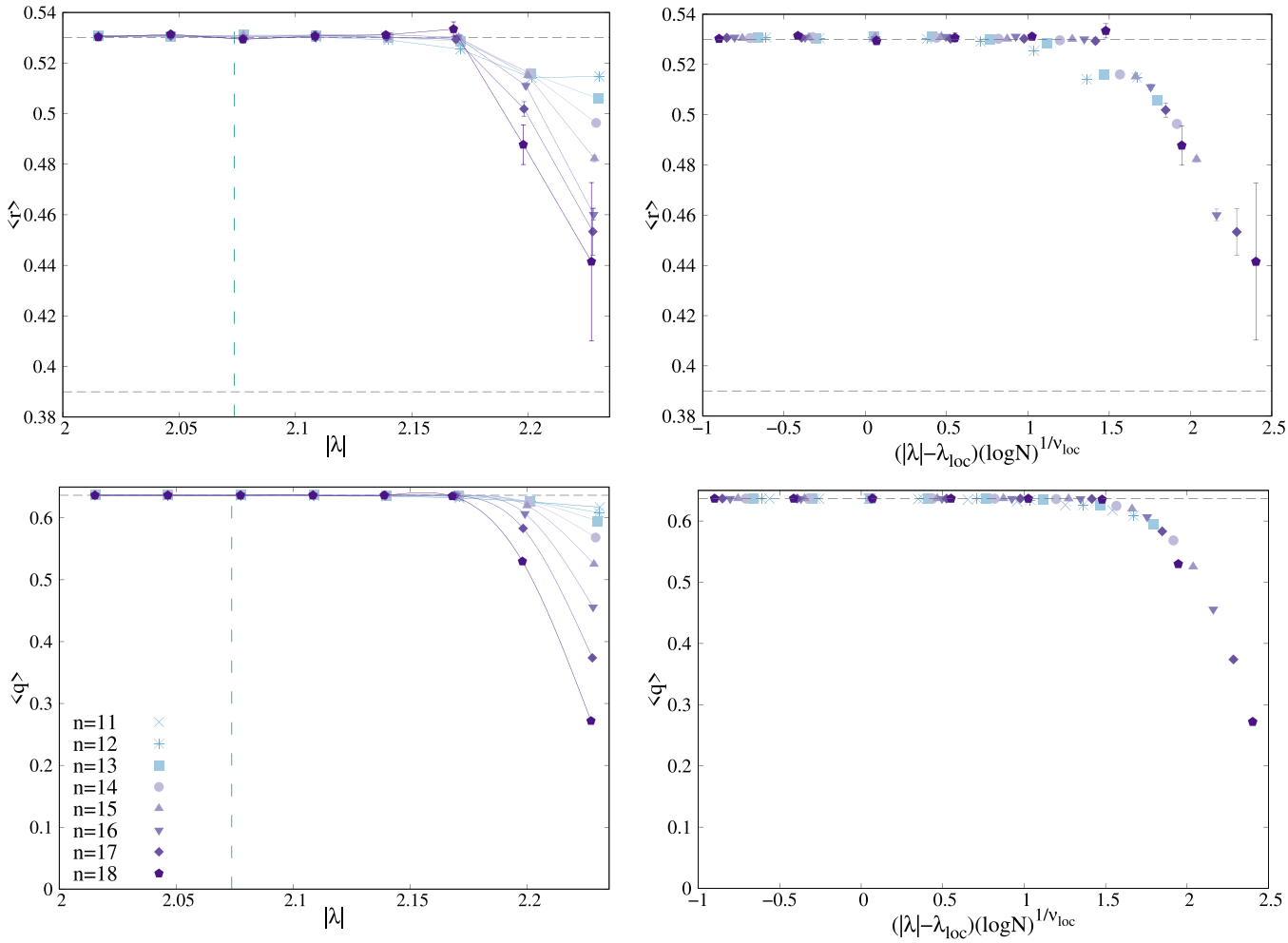

FIG. 4. $\langle r\rangle$ (top) and $\langle q\rangle$ (bottom) as a function of $|\lambda| \in (2, \lambda_{\max})$ in the tails of the spectrum of the adjacency matrix of critical ER graphs for $b = 0.5$ ($\lambda_{\max} \approx 2.231$). Different system sizes $N = 2^n$ (with n from 11 to 18) correspond to different symbols and colors as indicated in the legend. The right panels show that a good data collapse is obtained for both $\langle r\rangle$ and $\langle q\rangle$ in terms of the scaling variable $(\lambda - \lambda_{\rm loc})(\ln N)^{1/\nu_{\rm loc}}$, with $\lambda_{\rm loc} \approx 2.074$ [Eq. (7)] and $\nu_{\rm loc} \approx 1$. The horizontal dashed grey lines correspond the GOE and Poisson universal values.

observables take their Wigner-Dyson universal values for $\lambda \leqslant \lambda_{\rm loc}$, while they depart from the Wigner-Dyson values for $\lambda > \lambda_{\rm loc}$, in a way that is more pronounced when the system size is increased. The right panels demonstrate that a good collapse of the data (especially for $\langle q\rangle$ which turns out to be much less noisy than $\langle r\rangle$) corresponding to different sizes is obtained in terms of the scaling variable $(\lambda - \lambda_{\rm loc})(\ln N)^{1/\nu_{\rm loc}}$, with $\nu_{\rm loc} \approx 1$. (Such value of the exponent is the same found for the Gaussian RP model at the AL transition [76].) Here for concreteness we have used the estimation of $\lambda_{\rm loc}$ given by the Mott criterion, Eq. (7), i.e., $\lambda_{\rm loc} \approx 2.074$ for $b = 0.5$. A reasonably good collapse can be also obtained setting the mobility edge to the value given by the linear stability analysis of the approximate cavity equations, $\lambda_{\rm loc} \approx 2.045$ (see Sec. IV B) and using $\nu_{\rm loc} \approx 0.75$. It is also possible to collapse the data for different values of N on the same curve assuming that transition from Wigner-Dyson to Poisson statistics takes place at $\lambda_{\rm loc} = 2$ and setting $\nu_{\rm loc} \approx 0.5$. This situation would be realized either if the intermediate partially delocalized but nonergodic phase was only a finite-size crossover and eventually all eigenvalues in the tails of the spectrum become fully localized in the thermodynamic limit, or if the structure of the fractal states is different from the one of RP-type models, as it happens for instance in correlated random matrix models having a fractal phase that does not feature minibands in the local spectrum within which the Wigner-Dyson statistics establishes [66–68]. However the quality of the collapse in this case is slightly less good than the one achieved in the right panels of Fig. 4. To sum up, the finite-size scaling analysis of the level statistics is fully compatible with a transition from Wigner-Dyson to Poisson statistics at $\lambda_{\rm loc} > 2$, corroborating the results of the previous section. Yet, our numerical data are limited to too small sizes to rule out definitely other possible scenarios and to be fully conclusive on the nature of the transition.

Finally, the plots Fig. 4 call attention on an important difference with the standard AL transition on sparse graphs induced by the random local potential. In fact, in this case, it is well established that the critical point is in the localized phase and it is thus described by the Poisson statistics [6,7,11,13–15,112], while in the present case, the critical point lies clearly in the Wigner-Dyson phase. This latter behavior is also observed in random matrix models of the RP type featuring an intermediate nonergodic extended phase sand-

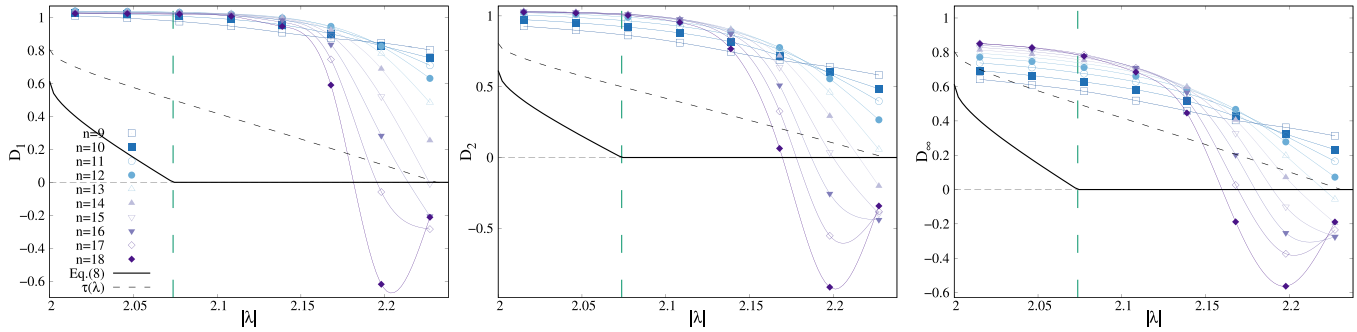

FIG. 5. Flowing N-dependent fractal dimensions D_1 (left), D_2 (middle), and D_∞ (right) as a function of $|\lambda| \in (2, \lambda_{\max})$ in the tails of the spectrum of the adjacency matrix of critical ER graphs for $b = 0.5$ ($\lambda_{\max} \approx 2.231$). $N = 2^n$ with $n = 9, \ldots, 18$ (different values of n correspond to different symbols and colors as indicated in the legend). D_q are computed via Eq. (18) from the scaling of the qth moment of the wave-function amplitudes measured from EDs. The error bars on D_q are smaller than the size of the symbols. The solid line corresponds to the analytic estimation based on the Fermi Golden Rule, Eq. (9). The vertical dashed line represents the position of $\lambda_{\rm loc} \approx 2.074$. The dashed curve shows the value of the exponent $\tau(\lambda)$ associated to the scaling of the DoS, which gives an upper bound for the anomalous dimensions [18].

wiched between the fully ergodic one and the fully localized one [56,76]. This observation thus provides another hint of the existence of a genuine partially delocalized but nonergodic phase in the tails of critical ER graphs.

B. Statistics of the wave-function amplitudes

We now focus on the transition for the statistics of the wave-function amplitudes taking place at $|\lambda| = \lambda_{\rm GOE} = 2$. To this aim, we study the scaling behavior of the (*typical*) moments

$$\Upsilon_q(N,\lambda) = \left\langle \ln\left(\sum_{i=1}^{N} |\psi(i)|^{2q}\right)\right\rangle_\lambda,$$
$$\Upsilon_1(N,\lambda) = -\left\langle \sum_{i=1}^{N} |\psi(i)|^2 \ln|\psi(i)|^2\right\rangle_\lambda, \qquad (17)$$

where the averages $\langle\cdots\rangle_\lambda$ are done over the eigenfunctions of energy λ and over different realizations of the graph. The flowing fractal dimensions are then obtained as logarithmic derivatives of the moments Υ_q with respect to $\ln N$ (hereafter the logarithmic derivatives are computed as discrete derivatives involving the five available values of the system size closest to N [113]):

$$D_q(N,\lambda) = \frac{1}{1-q}\frac{\partial \Upsilon_q(N,\lambda)}{\partial \ln N},$$
$$D_1(N,\lambda) = \frac{\partial \Upsilon_1(N,\lambda)}{\partial \ln N}. \qquad (18)$$

In Fig. 5, we plot our numerical results for the flowing fractal exponent $D_q(N,\lambda)$ computed numerically according to Eq. (18), and contrast it with the theoretical prediction of the Mott's argument based on the generalization of the Fermi Golden rule, Eq. (9). The figure shows that for $|\lambda| > \lambda_{\rm loc}$ the exponents D_1, D_2, and D_∞ start to decrease rapidly as the system size is increased (and even take negative values). Conversely, for $|\lambda| < \lambda_{\rm loc}$, D_q are still quite close to 1 (and are still larger than τ). Attempting a finite-size scaling analysis of these data is problematic due to the fact that D_q should converge to a λ-dependent function.

This kind of behavior is somewhat similar to the one observed in the insulating side of the MBL transition [43,48] (and also in the intermediate phase of the Lévy RP ensemble [56]), in which the asymptotic values of D_q depend continuously on the parameters of the model such as the disorder strength. We therefore perform a finite-size scaling analysis inspired by the one proposed in Refs. [43,56,114] to deal with this situation, which consists in positing that in the partially delocalized but nonergodic region, $|\lambda| \in (\lambda_{\rm GOE}, \lambda_{\rm loc})$, the moments of the wave-function amplitudes $\langle\Upsilon_q\rangle$ [defined in Eq. (17)] behave as

$$\Upsilon_1(N,\lambda) - \Upsilon_1(N,\lambda=2) = -D_{1,c}\frac{\ln N}{\xi(\lambda)},$$
$$\Upsilon_q(N,\lambda) - \Upsilon_q(N,\lambda=2) = (1-q)D_{q,c}\frac{\ln N}{\xi(\lambda)}, \qquad (19)$$

with $D_{q,c}$ being the fractal dimensions at the transition point. The length scale ξ (i.e., the logarithm of a correlation volume $N_c(\lambda)$) depends on the distance to the critical point $\lambda_{\rm GOE} = 2$. The scaling ansatz above implies that in the limit $\ln N \gg \xi$ the leading terms follows $\Upsilon_1 \simeq D_{1,c}(1 - 1/\xi(\lambda))\ln N$ and $\Upsilon_q \simeq -(q-1)D_{q,c}(1-1/\xi(\lambda))\ln N$, while in the opposite limit, $\ln N \ll \xi$, one retrieves the critical scaling. As mentioned above, here for simplicity, in analogy with the RP model [52], we assume that the minibands in the local spectrum in the partially delocalized but nonergodic phase are fractal but non *multi*fractal, i.e., $D_q = D$ for all q. In order for Eq. (9) to be satisfied one then needs to have

$$\xi(\lambda) = \frac{D_c}{D_c - D(\lambda)}, \qquad (20)$$

where $D_c = 1 - 2b/b_\star$ and $D(\lambda)$ is given in Eq. (9). As shown in Fig. 6 for $b = 0.5$, a reasonably good data collapse is obtained in the partially delocalized phase when the qth moments of the wave functions amplitudes for different values of the energy are plotted as a function of the scaling variable $\ln N/\xi(\lambda)$, where $\xi(\lambda)$ is chosen as in Eq. (20). Note that the quality of the data collapse is especially good since there is in fact *no adjustable parameter* in this procedure. Since $\tilde{\kappa}(2+\epsilon) \approx 2(1+\sqrt{\epsilon})$, in the vicinity of the transi-

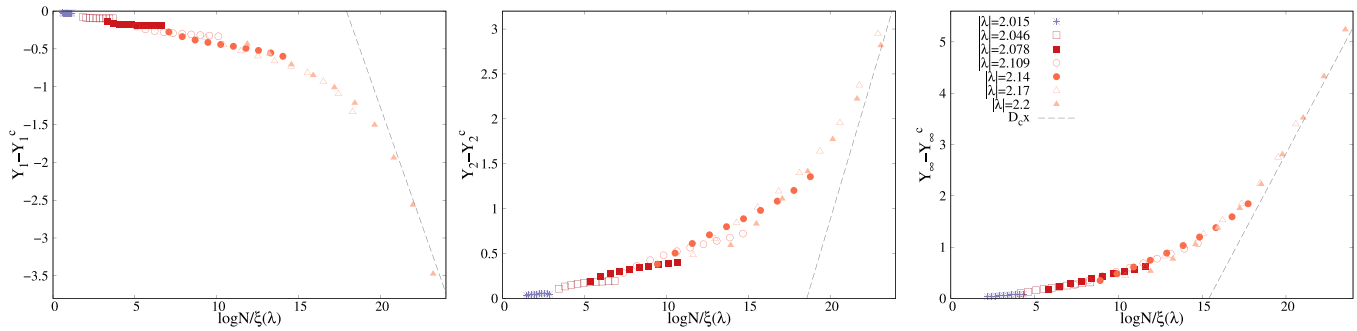

FIG. 6. Scaling curves for the qth moments of the wave-function amplitudes for $q = 1$ (left), $q = 2$ (middle), and $q = \infty$ (right) varying λ in the tails of the spectrum of the adjacency matrix of critical ER graphs for $b = 0.5$. Different colors and symbols correspond to different values of the energy. $\Upsilon_q(N, \lambda) - \Upsilon_q(N, \lambda = 2)$ are plotted as a function of the scaling variable $\ln N/\xi(\lambda)$, see Eq. (19) with ξ given by Eq. (20). The gray dashed lines correspond to the theoretical asymptotic behavior of the scaling functions that are predicted to exhibit a slope equal to $D_c = 1 - 2b/b_\star$. The error bars on Υ_q are smaller than the size of the symbols.

tion to the fully delocalized GOE like phase one has that $\tau(2+\epsilon) - \tau(2) \approx 2b \ln 2\sqrt{\epsilon}$. Hence the scaling analysis of Fig. 6 indicates that

$$\xi(\lambda) = \frac{b_\star - 2b}{2b(b_\star + 1)\sqrt{|\lambda| - 2}},$$

i.e., $\nu_{\mathrm{GOE}} = 0.5$.

An independent estimation of the exponent ν_{GOE} which describes how the correlation length scale $\xi(\lambda)$ diverges when the critical point is approached can be obtained from the nonmonotonic behavior of the flowing fractal dimensions D_q at fixed energy and as a function of the system size. In Fig. 7, we plot the numerical estimations of D_1, D_2, and D_∞ as a function of $n = \ln_2 N$ for several values of λ within the interval $2 < |\lambda| < \lambda_{\max}$. The plots show that the D_q's first grow at small N and then decrease at large N after passing through a maximum at a characteristic scale N_c. The position of the maximum moves to larger values of N when λ gets closer to 2. The values of $N_c(\lambda)$ estimated from the nonmonotonic behavior of the D_q's are shown in Fig. 8, indicating that the characteristic scale $\ln(N_c)$ governing the finite-size behavior of the fractal exponents is well fitted by a power-law divergence of the form $\ln(N_c) \propto (|\lambda| - 2)^{-\nu_{\mathrm{GOE}}}$ with $\nu_{\mathrm{GOE}} \approx 0.5$, and appears to be proportional to the correlation length $\xi(\lambda)$ extracted from the finite-size scaling analysis of Fig. 6.

It is also worth mentioning that we also tried to perform a finite-size scaling of the D_q and Υ_q assuming that there is a direct transition to localization at $\lambda_{\mathrm{loc}} = 2$ (and thus no intermediate phase), and that D_q tend to 0 in the thermodynamic limit for $|\lambda| > 2$. However we did not manage to find a good collapse of the data for any choice of the parameters. Hence, to sum up, the finite-size scaling analysis of the moments of the wave-function amplitudes presented above provides another element in support of the existence of the intermediate phase, and indicates that the transition from the fully delocalized phase in the bulk of the spectrum to the partially delocalized but nonergodic phase in the region $|\lambda| \in (2, \lambda_{\mathrm{loc}})$ is governed by a characteristic scale that diverges exponentially at $\lambda_{\mathrm{GOE}} = 2$.

C. Convergence of the average density of states

In this section, we investigate the convergence of the average DoS in the tails of the spectrum of the adjacency matrix of critical ER graphs to the exact asymptotic behavior obtained in Ref. [18] and given in Eq. (3). Although the average DoS is completely insensitive to AL, this analysis will allow us to obtain another complementary estimation of the characteristic scale that governs finite-size corrections. The numerical results are obtained using both exact diagonalizations (for sizes

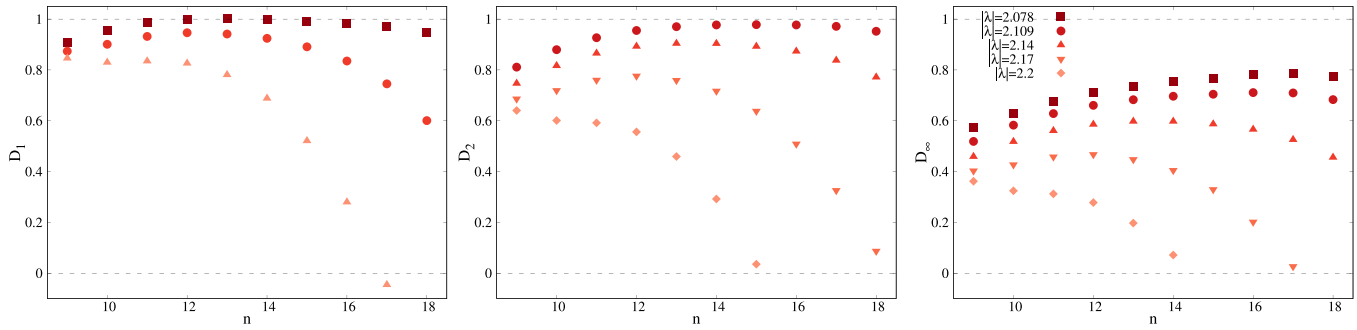

FIG. 7. Flowing fractal dimensions D_1 (left), D_2 (middle), and D_∞ (right) as a function of $n = \log_2 N$ for different values of $|\lambda| \in (2, \lambda_{\max})$ in the tails of the spectrum of critical ER graphs of N vertices and average degree $c = b \ln N$ with $b = 0.5$. Different symbols and colors correspond to different values of the energy as indicated in the legend. The fractal exponents exhibit a clear nonmonotonic dependence on n. The error bars on D_q are smaller than the size of the symbols.

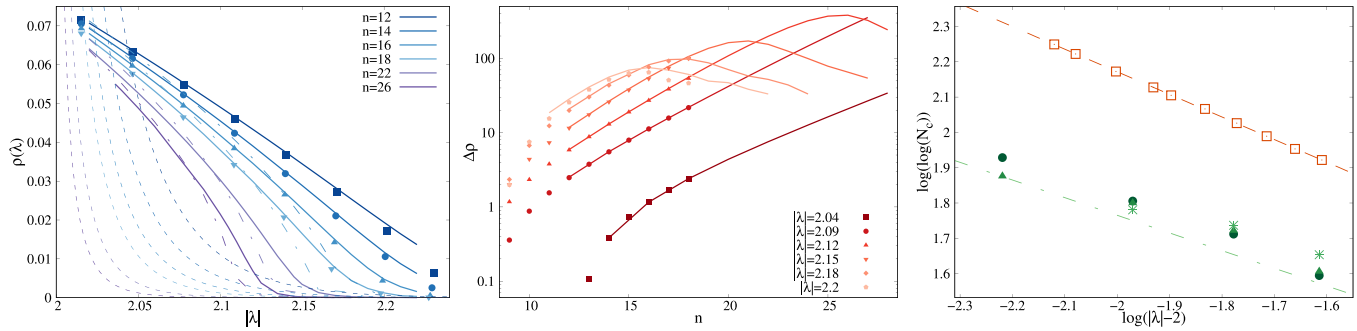

FIG. 8. (Left) Average DoS of critical ER graphs (with $b = 0.5$) in the semilocalized phase $|\lambda| \in (2, \lambda_{\max})$ computed using EDs (symbols) and the numerical solution of Eqs. (10) and (11) (thick continuous lines). $\lambda_{\max} \approx 2.231$ for $b = 0.5$. Different system sizes $N = 2^n$ (with n from 12 to 26) correspond to different symbols and colors as indicated in the legend. The dashed lines correspond to the asymptotic value of the DoS ρ^∞ given in Ref. [18] and in Eq. (3). The dashed-dotted lines corresponds to the approximate average DoS obtained from the solution of Eq. (13), which is in reasonably good agreement with the average DoS obtained from EDs and from the solution of the exact cavity equations. (Middle) Relative distance at finite N of the DoS from its asymptotic scaling behavior $\Delta\rho = (\rho - \rho^\infty)/\rho^\infty$ for several values of the energy in the interval $|\lambda| \in (2, \lambda_{\max})$ as a function of $n = \log_2 N$. Filled symbols correspond to ED results and solid lines to the results obtained from the solution of the cavity equations. Different symbols and colors correspond to different values of the energy as indicated in the legend. The curves exhibit a nonmonotonic behavior with a maximum at a characteristic volume $N_c(\lambda)$. (Right) $\ln\ln(N_c)$ as a function of the logarithm of the distance from the transition point, $\ln(|\lambda| - 2)$. The empty squares correspond to the values of N_c extracted from the maximum of $\Delta\rho$, and are very well fitted by $\ln\ln N_c = a - \nu_{\rm GOE} \ln(\lambda - 2)$ with $a \approx 0.891$ and $\nu_{\rm GOE} \approx 0.64$ (dashed straight line). The filled circles, up triangles, and down triangles correspond to the values of N_c estimated from the nonmonotonic behavior of the flowing fractal dimensions D_1, D_2, and D_∞, respectively (see Fig. 7). The dashed-dotted line represents the estimation of $\xi \propto (|\lambda| - 2)^{-1/2}$ given in Eq. (20) (with $\nu_{\rm GOE} = 0.5$) obtained from the scaling analysis of the moments of the wave functions amplitudes proposed in Fig. 6 of Sec. V B.

$N = 2^n$ with $9 \leqslant n \leqslant 18$) and the numerical solution of the self-consistent cavity equations for the Green's function (for sizes $N = 2^n$ with $12 \leqslant n \leqslant 28$). In both cases, we have set $b = 0.5$.

In the left panel of Fig. 8, we plot the average DoS in the interval $2 < |\lambda| < \lambda_{\max}$ for several system sizes obtained from EDs (symbols) and the cavity method (solid lines) for $b = 0.5$. We also plot the exact asymptotic estimation of Eq. (3) obtained by counting the number of vertices of abnormally large degree corresponding to a given energy (dashed lines) [18], as well as the estimation of the average DoS obtained from the approximate treatment of the cavity equations, Eq. (13) (dashed-dotted lines).

The first important observation is that the results obtained using the cavity method are in excellent agreement with the ED ones, although the DoS is still very far from the asymptotic expression (3) for the accessible system sizes. We also note that the approximate DoS obtained from Eq. (13) provides in fact a reasonably good approximation. In order to characterize the finite-size corrections it is instructive to compute the relative distance between the measured DoS at finite N from the asymptotic value ρ^∞. In the right panel of Fig. 8, we plot $\Delta\rho = (\rho - \rho^\infty)/\rho^\infty$ as a function of $n = \ln_2 N$ for several values of the energy in the interval $2 < |\lambda| < \lambda_{\max}$. The plot clearly shows that $\Delta\rho$ has a nonmonotonic behavior as a function of N characterized by a well-defined maximum that becomes higher and moves to larger values of N as the energy is decreased. This implies that the finite-size corrections become stronger and stronger as the transition from the semilocalized phase and the fully delocalized one is approached, and are governed by a characteristic volume that grows when λ gets close to the transition point at $|\lambda| = \lambda_{\rm GOE} = 2$. By determining the position of the maximum of $\Delta\rho$ for different values of λ, one thus obtains a direct estimation of the correlation volume $N_c(\lambda)$, which is shown in the right panel of Fig. 8. It turns out that N_c is well fitted by a an exponential divergence at the transition point of the form $\ln N_c(\lambda) \propto (\lambda - 2)^{-\nu_{\rm GOE}}$, with $\nu_{\rm GOE} \approx 0.64$. The plot also indicates that such estimation of N_c is roughly proportional to the one obtained from the nonmonotonic behavior of the flowing fractal dimensions and from the finite-size scaling analysis of Fig. 6.

It is also instructive to study the evolution with the system size of the average DoS restricted to the nodes with degree k (with $k > 2c$), $\langle {\rm Im}G\rangle_k$. This quantity, which can be easily computed numerically from the solution of the self-consistent cavity equations for the resolvent, is plotted in Fig. 9 for two values of the energy in the interval $|\lambda| \in (2, \lambda_{\max})$ as a function of $\Lambda(k/c)$ (i.e., the value of the energy which in the thermodynamic limit is associated with vertices of degree k) for several system sizes $n = \log_2 N$ with $16 \leqslant n \leqslant 28$. These plots show that the correlation volume N_c also reflects in the finite-size behavior of $\langle {\rm Im}G\rangle_k$. In fact, according to the rigorous results of Refs. [18,21], in the thermodynamic limit $\langle {\rm Im}G\rangle_k$ should approach a narrowly peaked function around λ (vertical dashed lines), due to the bijection between resonant vertices of degree greater than $2c$ and eigenvalues larger than 2. For the accessible system sizes, we observe that $\langle {\rm Im}G\rangle_k$ exhibits a maximum located around values of $\Lambda(k/c)$ smaller than λ. The position of the maximum moves first slightly leftwards for $N < N_c(\lambda)$, and then slightly rightwards for $N > N_c(\lambda)$, while the function becomes more peaked as the system size is increased. In the left panel, we also show the results obtained for $\lambda = 2.09$ using the approximation of Eqs. (12) and (13) (dashed curves), which in fact describe qualitatively well the evolution of $\langle {\rm Im}G\rangle_k$ with the system size. The same approximation cannot be used for $\lambda = 2.135$ since the system enters in the localized regime $[N > N_{\rm loc}(\lambda)]$

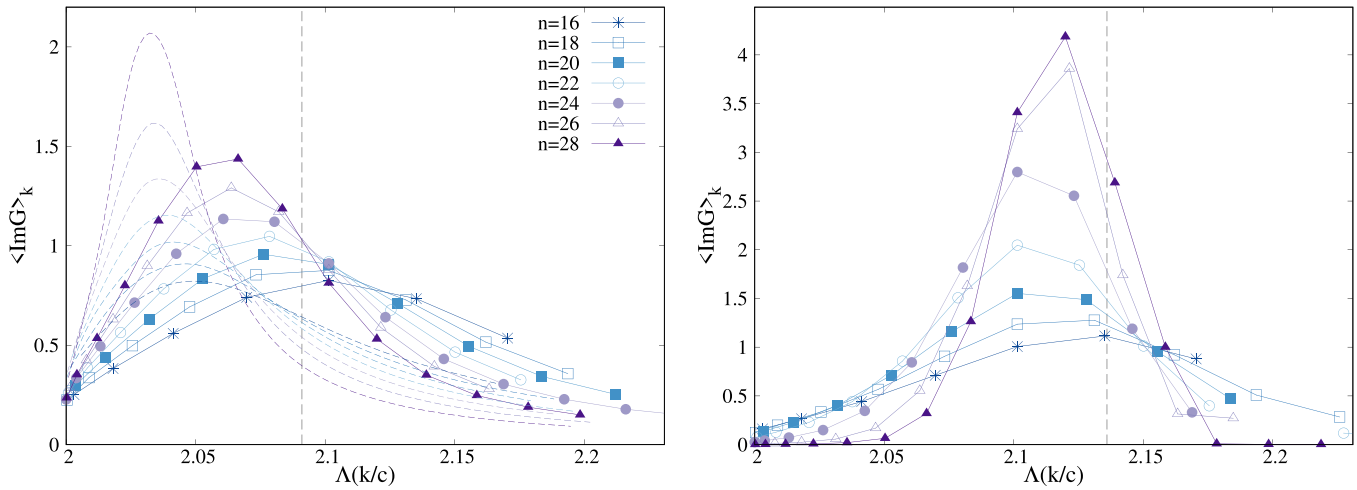

FIG. 9. Average DoS restricted to vertices of degree k, $\langle \mathrm{Im}G\rangle_k$, as a function of $\Lambda(k/c)$, in the tails of the spectrum of critical ER graphs (with $b = 0.5$). Different system sizes $N = 2^n$ (with n from 16 to 28) correspond to different symbols and colors as indicated in the legend. The vertical dashed lines corresponds to the value of the corresponding energy, i.e., $\lambda = 2.09$ (left) and 2.135 (right). The dashed curves in the left panel show $\langle \mathrm{Im}G\rangle_k$ obtained using the approximation of Eqs. (12) and (13).

in which the approximation breaks down, as explained in Sec. IV B.

All in all, the results presented above indicate the presence of a correlation volume, $N_c(\lambda)$, which diverges exponentially fast when $|\lambda| \to 2$ with an exponent close to $\nu_{\mathrm{GOE}} \approx 0.5$. Note that a similar divergence is also observed on the delocalized side of the Anderson model on the Bethe lattice [8–13,15,111,112,114]. In this case, the volumic scaling is associated to the fact that the critical point is in the localized phase and the fractal dimensions exhibit a discontinuous jump at the critical point from $D_q = 0$ for $W \geqslant W_c$ to $D_q = 1$ for $W \to W_c^-$. For critical ER graphs, the situation is somehow reversed, in the sense that here the critical point at $\lambda = 2$ is in the delocalized phase, with a finite jump of the fractal dimensions from $D_q = 1$ for $|\lambda| \leqslant 2$ to $D_q < 1$ for $|\lambda| \to 2^+$, and the scaling in terms of an exponentially large correlation volume is found on the semilocalized side of the transition [56].

D. Statistics of the local density of states through the mobility edge

The transition from the partially delocalized phase to the fully localized one can be also inspected by analyzing numerically the spectral statistics of the LDoS and of its correlations. Throughout this section, we will consider critical ER graphs with average degree $c = b \ln N$ with $b = 0.5$.

In Fig. 10, we plot the probability distribution $Q(\ln(\mathrm{Im}G))$ obtained solving the self-consistent cavity equations (10) and (11) for several system sizes $N = 2^n$ and for two values of the energy respectively in the putative partially delocalized but nonergodic phase ($\lambda = 2.04$, left panel) and in the fully localized phase ($\lambda = 2.135$, middle panel). The imaginary regulator η is set here to a very small value ($\eta = 10^{-16}$), much smaller than the mean level spacing. For $\lambda = 2.135$, the probability distribution of the LDoS seems to approach slowly but gradually the standard localized behavior as N is increased. In particular, one clearly observes the emergence of a power-law regime which becomes broader and broader as N is increased and is characterized by an exponent which evolves with N. The power-law establishes between the typical value of the LDoS (which drifts to smaller values when N is increased) and a sharp cutoff (that drifts to larger values as N is increased). In order to characterize the exponent of the power-law, in the right panel of Fig. 10, we plot the local slope of the distribution function, computed numerically as

$$\mu(\ln(\mathrm{Im}G)) = \frac{\partial Q(\ln(\mathrm{Im}G))}{\partial(\ln(\mathrm{Im}G))}.$$

In the standard localized regime, the tails of the distribution of the LDoS are described by $Q(\mathrm{Im}G) \propto \sqrt{\eta}/(\mathrm{Im}G)^{3/2}$ (for $\mathrm{Im}G$ smaller than a cut-off proportional to η^{-1}), i.e., $\mu = -1/2$. The figure indeed shows that as N is increased the region where μ is approximately constant becomes broader and the values of μ slowly increases towards $\mu = -1/2$ (dashed lines).

This behavior must be contrasted with the one of the partially delocalized phase, shown in the left panel of Fig. 10. For $\lambda = 2.04$, one indeed observes (at least for the accessible system sizes) that the typical value and the cut-off of the distributions of the LDoS stay of order 1 as N is increased and, albeit an apparent power-law regime seems to set in for large enough N, the exponent μ is much smaller than $-1/2$ and decreases with N. We also show the approximate result for $Q(\ln(\mathrm{Im}G))$ obtained from Eqs. (12)–(14), that in fact accounts reasonably well for the exact distributions in this regime.

It is also instructive to inspect the scaling behavior of the typical value of the LDoS as a function of the system size when the imaginary regulator is varied. In fact, as discussed in Refs. [52,56,73,74] in the context of random matrix models, in the putative partially delocalized but nonergodic phase eigenstates occupy a subextensive fraction of the total volume and spread over N^D nearby energy levels hybridized by the off-diagonal perturbation. Assuming for simplicity that

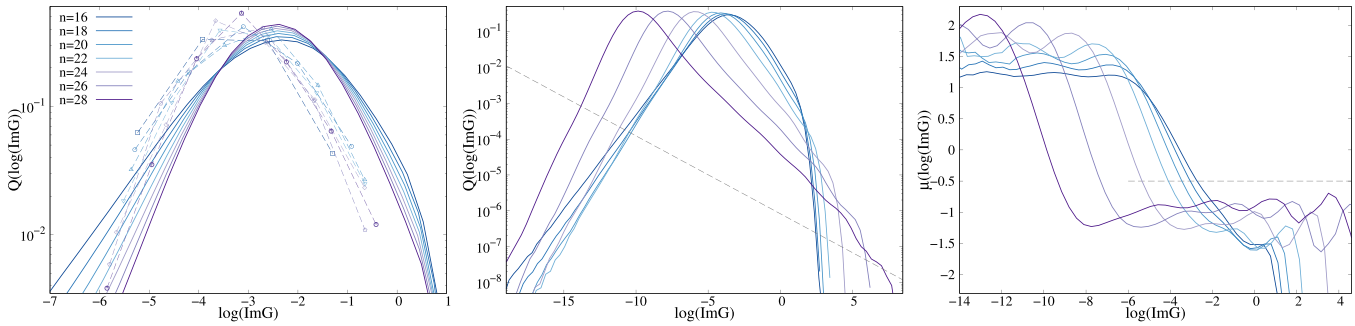

FIG. 10. Probability distribution functions of $\ln \mathrm{Im}G$ for critical ER graphs (with $b = 0.5$) for $\lambda = 2.04$ (left) and $\lambda = 2.135$ (right) and for several system sizes $N = 2^n$ with $n = 16, \ldots, 28$ as indicated in the legend. The dashed straight line in the middle panel represents the slope $\mu = -1/2$ of the standard localized phase. In the right panel, we plot the local slope of the probability distribution $\mu(\ln(\mathrm{Im}G))$, as explained in the text.

the minibands are locally compact (as in the Gaussian RP model [52,73,74]) the with of the minibands, i.e., the Thouless energy $E_{\mathrm{Th}} \equiv \Gamma$, is given by the product of the number of sites over which the eigenvectors are delocalized times the typical distance between consecutive levels: $E_{\mathrm{Th}} \propto N^D \Delta = N^D/(N\rho)$. At this energy scale the spectral statistics displays a crossover from a behavior characteristic of standard localized phases to a behavior similar to the one of standard delocalized phase. AL occurs when the minibands' width formally becomes smaller than the mean level spacing, $E_{\mathrm{Th}} \sim \Delta$. At this point, typically the localization centers are almost unaffected by the off-diagonal hybridization rates. [Conversely, full ergodicity is restored when the Thouless energy becomes of the order of the total spectral bandwidth, $E_{\mathrm{Th}} \sim O(1)$.] Hence, the scaling behavior of the local resolvent statistics encodes useful information on the structure of the local spectum and gives direct access to the support set of the minibands.

In Fig. 11, we plot the logarithm of the typical value of the LDoS, defined as

$$\rho_{\mathrm{typ}} = e^{\langle \ln \mathrm{Im}G \rangle} / \langle \mathrm{Im}G \rangle.$$

We have computed ρ_{typ} numerically by solving the self-consistent cavity equations (10) and (11) for several values of the regulator η, for several system sizes $N = 2^n$ (with n from 16 to 28), and for two values of the energy respectively in the putative partially delocalized but nonergodic phase ($\lambda = 2.07$, top-left panel) and in the fully localized phase ($\lambda = 2.135$, top-right panel). The imaginary regulator is measured in units of the mean level spacing $\Delta = 1/(N\rho(N,\lambda)) = \pi/(N\langle \mathrm{Im}G(\eta \to 0^+)\rangle)$. The curves corresponding to different size display a crossover at a well defined energy scale from a plateau at small η and a power-law of the form $\rho_{\mathrm{typ}} \propto (\eta/\Delta)^\beta$ at large η. As explained above the origin of such crossover is due to the fact that wave functions close in energy are hybridized by the off-diagonal perturbation and form minibands. When η is smaller than the width of the minibands ρ_{typ} has a delocalized-like behavior and is independent of the regulator. Conversely, when η is larger than the energy spreading of the minibands one finds a behavior similar to that of the localized phase, where ρ_{typ} grows with η.

At large energy ($\lambda = 2.135$, top-right panel), the ratio E_{Th}/Δ and the height of the plateau behave nonmonotonically as they first increase for $N < N_c$, and than start to decrease for $N > N_c$. The characteristic size $N_c \approx 2^{23}$ turns out to be precisely the one highlighted in Sec. V C. At larger N, one clearly sees that the ratio E_{Th}/Δ moves to smaller and smaller values and eventually for $N \gtrsim 2^{26}$ crosses the vertical dashed line, i.e., the Thouless energy becomes smaller than the mean level spacing. Concomitantly, the height of the plateau at small η decreases rapidly with the system size. This behavior is fully consistent with that of a fully localized regime.

At smaller energy, instead ($\lambda = 2.07$ in the putative partially delocalized but nonergodic phase, top-left panel), the ratio E_{Th}/Δ moves to larger and larger values as N is increased. This behavior is compatible with the presence of minibands in the local spectrum, at least for the accessible system size. In the left panel, we also show the approximate result for ρ_{typ} obtained using the approximate treatment of the cavity equations, Eqs. (12) and (13). Although this approximation clearly overestimates the typical DoS in the small η regime, it captures very accurately the crossover energy scale.

Another insightful probe of the level statistics and of the statistics of wave-function amplitudes is provided by the spectral correlation function $K_2(\omega)$ between eigenstates at different energy, which allows one to distinguish between ergodic, localized, and partially delocalized states [52,54,56,115–118]:

$$K_2(\omega) = \lim_{\eta \to 0^+} \left\langle \frac{N \sum_i \mathrm{Im}G_{ii}(\omega/2)\, \mathrm{Im}G_{ii}(-\omega/2)}{\sum_i \mathrm{Im}G_{ii}(\omega/2) \sum_i \mathrm{Im}G_{ii}(-\omega/2)} \right\rangle. \quad (21)$$

The properties of $K_2(\omega)$ and its relationship with other spectral probes have been discussed extensively in the literature (see, e.g., Ref. [118] for a review). For GOE matrices, $K_2(\omega) = 1$ identically, independently of ω on the entire spectral bandwidth. In a standard metallic phase (e.g., in the extended phase of the Anderson tight-binding model in $d \geqslant 3$), $K_2(\omega)$ has a plateau at small energies, for $\omega < E_{\mathrm{Th}}$, followed by a fast-decay which is described by a power-law, with a system-dependent exponent [116]. The height of the plateau is larger than one, which implies an enhancement of correlations compared to the case of independently fluctuating Gaussian wave functions. The Thouless energy which separates the plateau from the power-law decay stays finite in the thermodynamic limit and extends to larger energies as one goes deeply into the metallic phase, and corresponds to the energy band over which GOE-like correlations establish [115]. In a partially delocalized but nonergodic

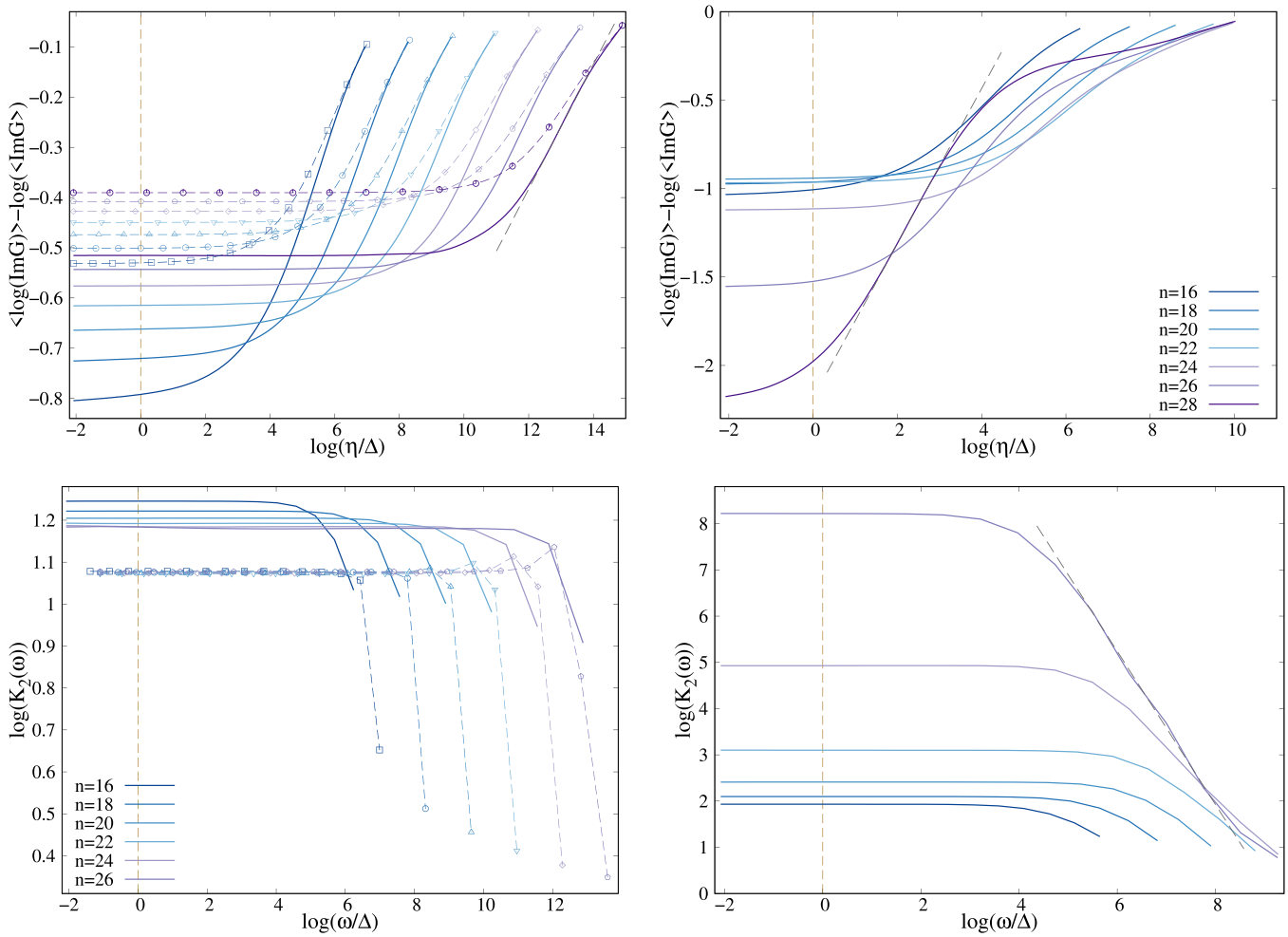

FIG. 11. (Top) Logarithm of the typical DoS, $\langle \ln \mathrm{Im}G\rangle - \ln\langle \mathrm{Im}G\rangle$, as a function of the imaginary regulator η divided by the mean level spacing $\Delta = \pi/(N\langle \mathrm{Im}G(\eta \to 0^+)\rangle)$, for to critical ER graphs (with $b = 0.5$) of size $N = 2^n$ (with n from 16 to 28 as indicated in the legend), for $\lambda = 2.07$ (top-left) and $\lambda = 2.135$ (top-right). The results obtained from the self-consistent solution of the cavity equations (10) and (11) are shown as continuous lines. The dashed lines represent the typical DoS obtained from the approximate treatment of the cavity equations, Eqs. (12) and (13). The dashed straight lines correspond to a fit of the form $\rho_{\mathrm{typ}} \propto (\eta/\Delta)^{\beta}$ ($\beta \approx 0.124$ for $\lambda = 2.07$ and $\beta \approx 0.438$ for $\lambda = 2.135$ for the largest available system size $N = 2^{28}$). Bottom panels: Logarithm of the overlap correlation function, Eq. (21), vs $\ln(\omega/\Delta)$ for critical ER graphs (with $b = 0.5$) of size $N = 2^n$, with $n = 16, \ldots, 26$ (different colors correspond to different value of n). In the bottom-left panel, $\lambda = 2.07$ and in the bottom-right panel, $\lambda = 2.135$. Continuous curves show the results obtained from the solution of the self-consistent cavity equations (10) and (11), while the dashed lines are obtained from the approximate treatment of Eqs. (12) and (13). The dashed straight line in the right panel shows a power law fit of the form $K_2(\omega) \propto \omega^{-\theta}$ (the exponent θ grows with N and $\theta \approx 1.66$ for the largest available system size $N = 2^{26}$).

phase, the plateau is present only in a narrow energy interval, as E_{Th} shrinks to zero in the thermodynamic limit still staying much larger than the mean level spacing. Beyond E_{Th} eigenfunctions poorly overlap with each other and the statistics is no longer Wigner-Dyson and $K_2(\omega)$ decay to zero [52,54,56].

Our numerical results are presented in the bottom panels of Fig. 11. The overlap correlation function is computed from the numerical solution of the self-consistent cavity equations for several values of the energy separation ω, for several system sizes ($N = 2^n$ with $16 \leqslant n \leqslant 26$), and for the same values of λ as above (and setting η to a very small value, $\eta = 10^{-16}$, much smaller than the mean level spacing).

At small enough energy ($\lambda = 2.07$ in the putative partially delocalized but nonergodic phase, bottom-left panel), $K_2(\omega)$ is constant for $\Delta < \omega < E_{\mathrm{Th}}$, reflecting the fact that the minibands are locally compact, as in the Gaussian RP model [52,56]. In agreement with the behavior of the typical DoS discussed above, we find that the ratio E_{Th}/Δ moves to larger and larger values as N is increased. At larger energy separation, $\omega \gg E_{\mathrm{Th}}$, eigenfunctions poorly overlap with each other, the statistics is no longer Wigner-Dyson and $K_2(\omega)$ decay fast to very small values. Again, we find that the approximate treatment of the cavity equations, Eqs. (12) and (13), provide a very accurate estimation of the Thouless energy.

In the fully localized phase ($\lambda = 2.135$, bottom-right panel), the ratio E_{Th}/Δ displays a nonmonotonic dependence on N, as discussed above. For $N \gg N_c \approx 2^{23}$, the Thouless energy eventually becomes smaller than the mean level spacing and a fully localized behavior is recovered. The plateau at small energy is followed by a fast decrease $K_2(\omega) \propto 1/\omega^{\theta}$.

VI. STATISTICS OF THE FLUCTUATION OF THE LARGEST EIGENVALUE

In this section, we analyze the statistics of the fluctuations of the largest (non trivial) eigenvalue of the laplacian of critical ER graphs whose asymptotic distribution, as mentioned in the introduction and as discussed in Ref. [20] in great details, is given by a law that does not match with any previously known distribution and does not satisfy the conclusion of the FisherTippettGnedenko theorem. [Note that we do not consider here the largest Perron-Frobenius eigenvalue of $\mathcal{H}$ associated to the flat eigenvector $1/\sqrt{N}(1,\ldots,1)$, which is an outlier separated from the rest of the spectrum, see, e.g., Ref. [16]].

As shown in Ref. [20], $\lambda_{\max}$ corresponds to the largest degree of $\mathcal{H}$ and its fluctuations can be computed in terms of the fluctuations of the largest value of N i.i.d. Poisson variables of average $c = b \ln N$. The probability that $k_{\max} = k$ can be esily expressed in terms of the cumulative distribution of the degree probability $R(k) = \sum_{k'=0}^{k} P(k')$:

$$\Psi(k_{\max}) = [R(k_{\max})]^N - [R(k_{\max} - 1)]^N. \tag{22}$$

By changing variable from $k_{\max}$ to $\lambda_{\max}$ via the bijection $\lambda_{\max} = \Lambda(k_{\max}/c)$ one immediately obtains the probability distribution function of the largest eigenvalue:

$$\Phi(\lambda_{\max}) = c\, \Psi(c\tilde{\kappa}(\lambda_{\max}))\, \tilde{\kappa}'(\lambda_{\max}). \tag{23}$$

We have computed $\Phi(\lambda_{\max})$ for critical ER graphs (with $b = 0.5$) both analytically, using Eqs. (22) and (23) for large $N \lesssim 2^{40}$, and numerically, using the Lanczos algorithm for the two largest eigenvalues of the adjacency matrix for $2^{16} \leqslant N \leqslant 2^{26}$. The results are shown in Fig. 12. We empirically find that the data corresponding to different N nicely collapse on the same curve if $\lambda_{\max} - \langle\lambda_{\max}\rangle$ is multiplied by $(\ln N)^{\alpha}$, with $\alpha = 3/4$. The right tails of the distribution are well represented by an exponential decay, while the left tails are much sharper, although there is no level repulsion with the eigenvectors on the left of $\lambda_{\max}$.

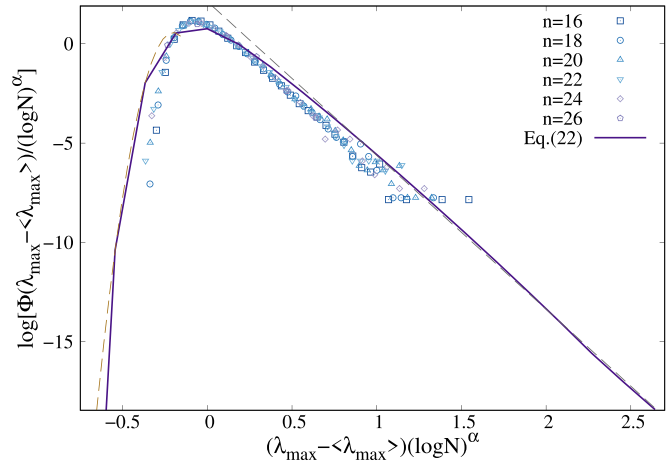

FIG. 12. Probability distribution of the largest eigenvalue (besides the one associated to the flat eigenvector) of the adjacency matrix of critical ER graphs with $b = 0.5$. Different symbols and colors correspond to different system sizes $N = 2^n$ as indicated in the legend. The data corresponding to different N collapse on the same curve when $\lambda_{\max} - \langle\lambda_{\max}\rangle$ is multiplied by $(\ln N)^{\alpha}$. The best collapse is achieved for $\alpha = 3/4$. The continuous curve correspond to the analytical expression obtained from Eqs. (22) and (23) for large $N = 2^{40}$. The right tails of the distribution of the largest eigenvalue are well fitted by an exponential decay (dashed straight line on the positive side), while the left tails are much sharper, and are possibly Gaussian (dashed curve on the negative side).

VII. RELATIONSHIP WITH THE OUT-OF-EQUILIBRIUM PHASE DIAGRAM OF THE QUANTUM RANDOM ENERGY MODEL

The QREM, is the quantum version of Derrida's random energy model [119] and provides the simplest toy model of mean-field spin glasses. For n spin-1/2s, it is defined by the following Hamiltonian:

$$\mathcal{H}_{\rm qrem} = E\left(\{\hat{\sigma}_i^z\}\right) - \Gamma \sum_{i=1}^{n} \hat{\sigma}_i^x, \tag{24}$$

where Γ is the transverse field, and $E(\{\hat{\sigma}_i^z\})$ is a random operator diagonal in the $\{\hat{\sigma}_i^z\}$ basis, which takes 2^n different values for the 2^n configurations of the n spins in the z-basis, identically and independently distributed according to

$$P(E) = \frac{e^{-E^2/n}}{\sqrt{\pi n}}.$$

With this choice of the scaling, the random many-body energies are with high probability contained in the interval $[-n\sqrt{\ln 2}, +n\sqrt{\ln 2}]$ in the thermodynamic limit. Hereafter we denote by $\varepsilon = E/n$ the intensive energy per spin corresponding to the extensive energy E.

As discussed above, the QREM can be viewed as the simplest many-body model that displays AL in its Hilbert's space: If one chooses as a basis the tensor product of the simultaneous eigenstates of the operators $\hat{\sigma}_i^z$, the Hilbert space of the many-body Hamiltonian is a n-dimensional hypercube of $N = 2^n$ sites and degree n. One can map a configuration of n spins to a corner of the n-dimensional hypercube by considering $\sigma_i^z = \pm 1$ as the top/bottom face of the cube's ith dimension. The random part of the Hamiltonian is by definition diagonal on this basis, and gives uncorrelated random energies on each site orbital of the hypercube: At $\Gamma = 0$ the many-body eigenstates of Eq. (24) are simply product states of the form $|\sigma_1^z\rangle \otimes |\sigma_2^z\rangle \otimes \cdots \otimes |\sigma_n^z\rangle$, and the system is fully localized. The interacting part of the Hamiltonian acts as single spin flips on the configurations $\{\sigma_i^z\}$, and plays the role of the hopping rates connecting "neighboring" sites in the configuration space. The many-body quantum dynamics is then recast as a single-particle noninteracting tight-binding Anderson model for spinless electrons in a disordered potential living on the 2^n corners of an hypercube in n dimensions (and degree n), with the spin configurations being "lattice sites," and the transverse field playing the role of the hopping amplitude between neighboring sites.

The out-of-equilibrium phase diagram of the QREM has been analyzed in great details in several recent papers [34–38,120,121]. At low enough transverse field, the DoS is controlled by the random on-site energies, $\rho_{\rm qrem}(\varepsilon) \simeq$

$P(\varepsilon) = \sqrt{n/\pi}\, e^{-n\varepsilon^2}$, and strongly concentrate around zero energy density in the thermodynamic limit, as naturally expected for many-body systems. Using the same notation as before, one has that for $|\varepsilon| > 0$ the DoS scales as $\rho_{\rm qrem}(\varepsilon) \propto N^{\tau(\varepsilon)-1}$, with $\tau(\varepsilon) = 1 - \varepsilon^2/\ln 2$. Hence, the vast majority of the states are found in the bulk of the spectrum that concentrates around $\varepsilon = 0$, while a small subextensive fraction of them are in the tails, in the interval $0 < |\varepsilon| < \sqrt{\ln 2}$.

As it is apparent from the analysis of Refs. [34–38], in the localized phase the local structure of an eigenvector of the QREM model is similar to that of the critical ER graph described above: exponentially decaying around well-separated localization centres associated with resonances of energy ε of the eigenvector. In the QREM, the localization centers arise from exponentially rare vertices with exceptionally large local values of the potential, while in the critical ER graphs the localization centers correspond to exponentially rare vertices of abnormally large connectivity. The only difference between the two models is the specific geometrical structure of the underlying graph, since the hypercube contains much more short loops compared to the ER graph. There are in fact $r!$ paths of length r connecting two nodes of the hypercube which correspond to spin configuration that differ by r spin flips, but this can be essentially recast as an effective renormalization of the hopping amplitude.

The out-of-equilibrium phase diagram of the QREM is in fact qualitatively identical to the one proposed in Fig. 2 for critical ER graphs [34–38]. In the bulk of the spectrum, $|\varepsilon| \approx 0$, one finds a fully delocalized GOE-like phase; At very large energy, close to the spectral edges, $|\varepsilon| \in (\varepsilon_{\rm loc}, \sqrt{\ln 2})$, one finds a fully Anderson localized phase in which eigenvectors are exponentially localized around a single resonance. Finally, at intermediate energies, $\varepsilon \in (0, \varepsilon_{\rm loc})$ one has an intermediate partially delocalized but nonergodic phase in which distant localization centers on the hypercube partially hybridize due to the exponentially small tunneling rates between them, thereby producing multifractal eigenfunctions which occupy a diverging volume, yet an exponentially vanishing fraction of the total Hilbert space, with $0 < D_q < \tau(q)$.

VIII. CONCLUSIONS AND PERSPECTIVES

In this paper, we have analyzed both analytically and numerically the spectral properties of the tails of the spectrum of the adjacency matrix of critical ER graphs, i.e., when the average degree is of the order of the logarithm of the number of vertices.

In a series of recent inspiring papers, Alt, Ducatez, and Knowles have rigorously shown that these systems exhibit a "semilocalized" phase in the tails of the spectrum where the eigenvectors are exponentially localized on a subextensive fraction of nodes with anomalously large degree [18,20,21]. We have proposed two approximate analytical treatments to analyze this regime. The first is based on simple rules of thumb for localization and ergodicity, often referred to as the Mott's criteria. The second approach relies on an approximate treatment of the self-consistent cavity equation for the resolvent. Both approaches suggest that the semilocalized phase splits in fact in two different phases separated by a mobility edge. At large energy, close to the spectral edges, as already rigorously proven in Ref. [20], one finds a fully Anderson localized phase in which the eigenvectors are localized around a *unique* localization center and the statistics of the eiganvalues is described by the Poisson statistics. At intermediate energy, sandwiched between the fully delocalized GOE-like phase in the bulk, and the Anderson localized phase at the edges, we find a partially delocalized but nonergodic phase, in which the eigenstates spread over *many* resonant localization centers close in energy due to the hybridization of the exponentially decaying part of the wave functions. In this regime, the exponentially small tunneling amplitudes between far away localization centers is counterbalanced by the number of localization centers towards which tunneling can occur, and the system exhibits minibands in the local spectrum. The level statistics is therefore of Wigner-Dyson type up to an energy scale which is much smaller than 1 but stays much larger than the mean level spacing.

We have presented a numerical study of the finite size scaling behavior of several observables related to the spectral statistics that is compatible with the theoretical predictions and allows us to characterize the critical properties of the two transitions: The transition from the fully delocalized phase to the semilocalized one is accompanied by a correlation volume that diverges exponentially fast when the transition point is approached from above, $|\lambda| \to 2^+$, with an exponent $\nu_{\rm GOE} \approx 0.5$. The transition from Poisson to Wigner-Dyson statistics occurring at the AL threshold is instead associated to an exponent $\nu_{\rm loc} \approx 1$. This analysis also highlights the differences with respect to the standard AL on sparse random graphs induced by the disorder in the local potential. In fact, in this case, it is well established that the critical point belongs to the localized phase [6,7,11,13–15,112], while in the present case the critical point is described by the Wigner-Dyson statistics, as also found in random matrix models of the RP type which feature an intermediate partially delocalized but nonergodic phase [56,76].

Finally, we have characterized the statistics of the fluctuations of the largest eigenvalue, which are essentially controlled by the fluctuations of the largest degree in the network.

Since critical ER graphs provide an idealized representation of the topological features of the Hilbert space of generic interacting many-body systems, we believe the results presented here might give new insights on the understanding of the mechanisms that produce localized and multifractal wave functions even in more complex settings. In fact we put forward a direct correspondence between the phase diagram of critical ER graphs and the out-of-equilibrium phase diagram of the QREM, which is the simplest model featuring a many-body localization transition. In this respect, it might be useful to generalize the approximate treatment of the cavity equations proposed in Sec. IV B to similar situations in which wave functions are localized around many resonant nodes, such as, for instance, in the QREM.

Several important questions remain of course still open. The most important one is probably related to the possibility that the putative delocalized but nonergodic phase is only a finite-size crossover and eventually disappears in the thermodynamic limit. In fact, the estimation of the mobility edge based on the Mott criterion does not take into account

neither the effect of the loops nor of higher order terms in the perturbative expansion, while the approximate treatment of the cavity equations is also based on a quite drastic simplification in which the local fluctuations of the degree are completely neglected. The finite-size scaling analysis of the observables related to the spectral statistics presented in Fig. 4 is limited to too small sizes to rule out definitely this possibility. One might therefore wonder whether for very large sizes, i.e., $N \gg N_c(\lambda)$, eventually all the eigenvectors in the tails of the spectrum become fully localized. A similar crossover occurs for instance in the tight-binding Anderson model on random-regular graphs, where the existence of a genuine delocalized but nonergodic phase in the infinite size limit has been the subject of an intense debate in the latest years and has been strongly questioned by recent works [15,33,105,110–112,114,122–129]. Another important aspect concerns the structure of the fractal states. In fact, throughout this paper, we have assumed that the partially delocalized but nonergodic phase is analogous to the one found in RP-type models with uncorrelated entries [52–54,56,73,74]. On the other hand, there are several correlated random matrix models [66–68] in which the structure of the fractal states is quite different and do not feature, for instance, the formation of minibands within which the Wigner-Dyson statistics is established. In the tails of critical ER graphs, the energies of the localization centers of a given degree (which depend mostly on the degrees of the neighbors [18,21]) and the effective tunneling amplitudes between them (which depend mostly on their distances) are essentially uncorrelated. It is therefor natural to assume that RP models with iid elements provide the correct physical picture for the partially delocalized but nonergodic wave functions. Yet, it would be highly desirable to put our conclusions on a firmer and more rigorous ground and to provide more stringent numerical tests of the existence of the partially extended but nonergodic phase and of its nature.

Another important open question is related to the critical behavior for $b > b_{\rm loc}$. Indeed our analysis indicates that the intermediate partially delocalized but nonergodic phase only exists provided that b is smaller than $b_{\rm loc} = b_\star/2$ (see Fig. 2), while for $b \in (b_{\rm loc}, b_\star)$, one should observe a direct transition at $|\lambda| = 2$ from the fully delocalized phase in the bulk of the spectrum to a fully Anderson localized phase in the tails in which eigenvectors are exponentially localized around a unique localization node. In this case the critical properties of such transition might be different compared to the one observed at $b = 0.5$ and discussed in Sec. V, and it is natural to wonder whether at large b one recovers the standard critical behavior of AL on sparse random graphs induced by a quenched random potential.

The limit $b \to 0$ is also puzzling for two reasons, and deserves special attention. On the one hand, the exponents τ and D, which are predicted to exhibit a finite jump from 1 for $|\lambda| = 2$ to $1 - b/b_\star$ and $1 - 2b/b_\star$ respectively for $|\lambda| \to 2^+$, behave continuously at the transition from the fully delocalized GOE-like phase to the partially extended but nonergodic phase for $b \to 0$, which could result in a modification of the critical properties compared to the $b > 0$ case. On the other hand, we know from previous studies [88,94,95] that for c arbitrarily large but finite the spectrum of ER graphs is characterized by Lifshitz tails due to extremely rare fluctuations of the local degrees associated to fully localized eigenvectors, which, however, does not match with the $b \to 0$ limit of the phase diagram of Fig. 2.

Possibly the most interesting perspective for future work is to study how the addition of some amount of disorder in the local potential affects the spectral properties of critical ER graphs. On the one hand, one might expect that quenched on-site randomness might destabilize the partially delocalized phase by suppressing the effective tunneling rates between the far-away localization centers. On the other hand, since the Anderson tight-binding model on random graphs of fixed connectivity is already at the brink of developing a delocalized but nonergodic phase [15,33,53,54,105,110–112,114,122–129], the addition of strong fluctuations of the local degrees might in fact favor the formation of multifractal wave functions.

ACKNOWLEDGMENT

I would like to warmly thank I. M. Khaymovich, J. Alt, R. Ducatez, and A. Knowles for many enlightening and helpful discussions.

APPENDIX: UPPER BOUND ON THE POSITION OF THE MOBILITY EDGE

In this Appendix, we revise the rules of thumb criteria for localization and ergodicity discussed in Sec. IV A attempting to provide an upper bound on the position of the mobility edge and for the support set of the minibands.

In fact the matrix elements between the localization centers, Eq. (6), decay exponentially fast with the distance with a very high rate. One might then argue that the amplitudes $\mathcal{G}_r(\lambda)$ are dominated by the pairs of closest resonant localization centers. In the following we repeat the reasoning of Sec. IV A but, instead of using the typical distance between all pairs of localization nodes, $r_{\rm typ} = \ln N/\ln c$, to estimate the typical value of the tunneling rates, we take instead the minimal distance between pairs of nearby localization centers. This should provide a upper bound for $|\mathcal{G}_r(\lambda)|$ and hence for the position of the mobility edge as well as for the exponent D.

In order to compute the minimal distance between pairs of localization centers at a given energy λ, we start by evaluating the probability $P_\lambda(r)$ to find a localization center (at energy λ) at distance r from a given localization center (at the same energy) located at the origin. This is given by the probability that a ball of radius r around the origin (which roughly contains kc^{r-1} vertices) does not contain a localization center of energy λ times the probability to find one localization center exactly at distance r from the origin:

$$P_\lambda(r) \approx \rho(\lambda) k c^{r-1} (1-\rho(\lambda))^{kc^{r-1}} \approx \rho(\lambda)\tilde{\kappa}(\lambda) c^r e^{-\tilde{\kappa}(\lambda)\rho(\lambda)c^r},$$

where $k = c\tilde{\kappa}(\lambda)$ is the connectivity of the localization nodes which give rise to eigenstates of energy λ. From the expression above one immediately obtains the typical value of the distance between the two closest localization centers at energy

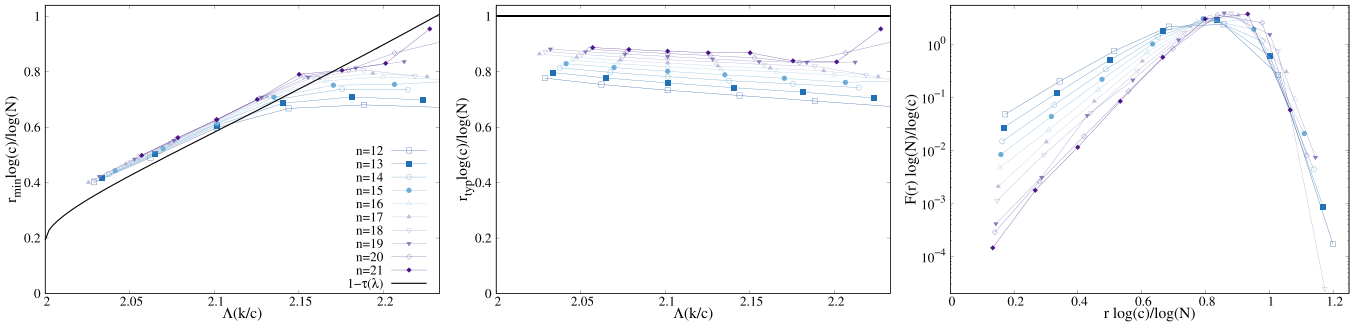

FIG. 13. Scaling behavior of the distance between localization centers for critical ER graphs with $b = 0.5$. In the left panel, we plot the typical value of the minimal distance between pairs of resonant localization centers of degree $k > 2c$. The data corresponding to different system sizes (as indicated in the legend) are divided by $\ln N/\ln c$ and are plotted as a function of the energy of the corresponding eigenstates $\Lambda(k/c)$. The solid line correspond to $1-\tau(\lambda)$, in agreement with the scaling given in Eq. (A1). In the middle panel, we plot the typical distance between all pairs of resonant localization centers of degree $k > 2c$ divided by $\ln N/\ln c$ as a function of the energy of the corresponding eigenstates $\Lambda(k/c)$ for the same values of N as before. Similar results are found for different values of b. In the right panel, we plot the probability distributions of the distances between pairs of localization nodes of fixed energies. In particular, we consider vertices of degree n within graphs of size $N = 2^n$, giving rise asymptotically to eigenvalues of energy $|\lambda| \approx 2.1014$ for $b = 0.5$. The distance r is rescaled by $\ln N/\ln c$.

λ as

$$r_{\min}(\lambda) \approx -\frac{\ln[\tilde{\kappa}(\lambda)\rho(\lambda)]}{\ln c}. \tag{A1}$$

Hence, for critical ER graphs, $r_{\min}$ scales in the thermodynamic limit as $r_{\min}(\lambda) \propto (1-\tau(\lambda))\ln N/\ln(b\ln N)$ minus a small λ-dependent correction proportional to $\ln\tilde{\kappa}(\lambda)/\ln(b\ln N)$. The origin of this correction comes from the fact that the volume of a ball of radius r around a localization center increases with the energy λ (i.e., the degree $c\tilde{\kappa}(\lambda)$ of the node). Note that for $\rho \to 0$, one has that $r_{\min}$ coincides with the radius of the ER graph $r_{\rm typ} = \ln N/\ln c$, while for $\rho \to 1$ the minimal distance becomes of order 1, as expected.

In order to check that the scaling obtained in Eq. (A1) is correct, we have computed numerically the typical value of the minimal distance between localization centers for critical ER graphs with $b = 0.5$ as explained below. We generate random instances of the adjacency matrix according to the probability distribution (1) and considered all the nodes of abnormally large connectivity $k > 2c$. For any given node of connectivity k [corresponding to a localization center of energy $\lambda = \Lambda(k/c)$], we measure the distance from its closest localization center of the same degree, and average this distance over all the nodes of degree k and over different random realizations of the graph. The results are reported in the left panel of Fig. 13, where this distance is plotted as a function of $\lambda = \Lambda(k/c)$. We see that the points corresponding to different sizes of the graph $n = \log_2 N$ collapse on the same curve corresponding to $1-\tau(\lambda)$ when rescaled by the factor $\ln N/\ln c$, in agreement with Eq. (A1). (Small deviations are observed for the smallest sizes at large λ, as explained above.) In the middle panel, we also plot the average distance between all pairs of nodes of degree k as a function of λ and for several values of N. We see that the data points corresponding to different sizes approach 1 when rescaled by the factor $\ln N/\ln c$, as expected. The origin of the finite-size corrections can be again understood recalling that nodes with abnormally large degree have $\tilde{\kappa}(\lambda)$ more neighbors at a given distance than the nodes with degree of order c. Finally, in the right panel of Fig. 13, we plot the whole probability distributions $F(r)$ of the distance between pairs of localization nodes of fixed energy for several sizes of the graph. In particular, we focus on vertices of degree n found within graphs of $N = 2^n$ nodes. Via the bijection (2) their energy corresponds asymptotically to $|\lambda| = \Lambda((b\ln 2)^{-1}) \approx 2.1014$ for $b = 0.5$. One clearly observes that, upon rescaling the distance r by $\ln N/\ln c$, the distributions are peaked around 1, as expected, and become more narrow as N is increased.

Inserting now the estimation of $r_{\min}$ (A1) into Eq. (6), the Mott criterion for full localization around a unique vertex yields $|G_{r_{\min}(\lambda)}(\lambda)| < (N\rho(\lambda))^{-1}$, i.e.,

$$N^{[\tau(\lambda)-(1-\tau(\lambda))(\frac{1}{2}+\frac{\ln\lambda}{\ln c})]} < 0.$$

In the thermodynamic limit (and in the critical regime, $c = b\ln N$), this condition is only fulfilled provided that $\tau(\lambda) < 1/3$. Using the asymptotic expression for the exponent τ given in Eq. (3), one then obtains a modified implicit equation for the mobility edge:

$$\tilde{\kappa}(\tilde{\lambda}_{\rm loc})[\ln\tilde{\kappa}(\tilde{\lambda}_{\rm loc}) - 1] = \frac{2}{3b} - 1. \tag{A2}$$

Since $\tau(\lambda)$ is a decreasing function of λ which tends to $1 - b/b_\star$ for $|\lambda| \to 2^+$, the existence of the partially delocalized but nonergodic phase is only possible if $b < \tilde{b}_{\rm loc} = 2b_\star/3 = 1/(\ln 8 - 3/2)$.

At this point, one can proceed further and compute the escape rate of a particle sitting on a localization center using $r_{\min}$ instead of $r_{\rm typ}$ in the expression of the transition rate, and compare it to the spectral bandwidth at the same energy. The Fermi golden rule gives

$$\Gamma(\lambda) \approx 2\pi N\rho(\lambda)|\mathcal{G}_{r_{\min}(\lambda)}(\lambda)|^2 \propto N^{2\tau(\lambda)-1}.$$

Assuming again for simplicity that this energy scale coincides with the number of hybridized states within a miniband times the mean level spacing, one obtains a direct estimation of the fractal exponent D as $\Delta N^D \propto \Gamma$, with $\Delta = 1/(N\rho)$, yielding $D = 3\tau - 1$ (note that $D = 0$ at the localization threshold where $\tau(\tilde{\lambda}_{\rm loc}) = 1/3$).

Since the number of localization centers is at most equal to $N\rho$, one has that D is at most equal to τ, and $D(\lambda) = \min\{\tau(\lambda), 3\tau(\lambda) - 1\}$. Hence, this argument predicts the existence of another transition at an energy $\lambda_{\rm ergo}$ within the tails of the spectrum from a phase, for $|\lambda| \in (2, \lambda_{\rm ergo}]$, where the wave functions spread uniformly over *all* the N^τ localization centers (i.e., $D = \tau$), to a nonergodic phase, for $|\lambda| \in (\lambda_{\rm ergo}, \tilde{\lambda}_{\rm loc})$, in which the wave functions only occupy a small fraction of the N^τ localization centers at that energy (i.e., D is strictly smaller than τ). The implicit equation for $\lambda_{\rm ergo}$ is given by the condition $\tau(\lambda_{\rm ergo}) = 1/2$, which is in fact the same condition that we obtained for the mobility edge when we used the typical distance between pairs of localization centers to evaluate the transition amplitudes, Eq. (7). Finally, this argument gives the following upper bound for the fractal exponent D in the thermodynamic limit:

$$D(\lambda) = \begin{cases} \tau(\lambda) & \text{for } 2 < |\lambda| < \lambda_{\rm ergo}, \\ 3\tau(\lambda) - 1 & \text{for } \lambda_{\rm ergo} < |\lambda| < \tilde{\lambda}_{\rm loc}, \\ 0 & \text{for } |\lambda| > \tilde{\lambda}_{\rm loc}. \end{cases}$$

[1] P. W. Anderson, Phys. Rev. **109**, 1492 (1958).
[2] A. Lagendijk, B. V. Tiggelen, and D. S. Wiersma, Phys. Today **62**(8), 24 (2009).
[3] P. A. Lee and T. V. Ramakrishnan, Rev. Mod. Phys. **57**, 287 (1985).
[4] F. Evers and A. D. Mirlin, Rev. Mod. Phys. **80**, 1355 (2008).
[5] R. Abou-Chacra, P. W. Anderson, and D. J. Thouless, J. Phys. C **6**, 1734 (1973).
[6] K. B. Efetov, Zh. Eksp. Teor. Fiz. **88**, 1032 (1985) [Sov. Phys. JETP **61**, 606 (1985)].
[7] K. B. Efetov, Zh. Eksp. Teor. Fiz. **92**, 638 (1987); **93**, 1125 (1987).
[8] A. Mirlin and Y. V. Fyodorov, J. Phys. A: Math. Gen. **24**, 2273 (1991).
[9] Y. V. Fyodorov and A. D. Mirlin, Phys. Rev. Lett. **67**, 2049 (1991).
[10] Y. V. Fyodorov, A. D. Mirlin, and H.-J. Sommers, J. Phys. I **2**, 1571 (1992).
[11] A. D. Mirlin and Y. V. Fyodorov, Nucl. Phys. B **366**, 507 (1991); Phys. Rev. B **56**, 13393 (1997).
[12] A. D. Mirlin and Y. V. Fyodorov, J. Phys. I **4**, 655 (1994).
[13] M. R. Zirnbauer, Phys. Rev. B **34**, 6394 (1986); Nucl. Phys. B **265**, 375 (1986).
[14] J. J. M. Verbaarshot, Nucl. Phys. B **300**, 263 (1988).
[15] K. S. Tikhonov and A. D. Mirlin, Phys. Rev. B **99**, 024202 (2019).
[16] G. Biroli, G. Semerjian, and M. Tarzia, Prog. Theor. Phys. Suppl. **184**, 187 (2010).
[17] M. Aizenman and S. Warzel, J. Math. Phys. **53**, 095205 (2012); Phys. Rev. Lett. **106**, 136804 (2011).
[18] J. Alt, R. Ducatez, and A. Knowles, Commun. Math. Phys. **388**, 507 (2021).
[19] J. Alt, R. Ducatez, and A. Knowles, arXiv:2109.03227.
[20] J. Alt, R. Ducatez, and A. Knowles, arXiv:2106.12519.
[21] J. Alt, R. Ducatez, and A. Knowles, Ann. Prob. **49**, 1347 (2021).
[22] B. L. Altshuler, Y. Gefen, A. Kamenev, and L. S. Levitov, Phys. Rev. Lett. **78**, 2803 (1997).
[23] D. M. Basko, I. L. Aleiner, and B. L. Altshuler, Ann. Phys. **321**, 1126 (2006).
[24] I. V. Gornyi, A. D. Mirlin, and D. G. Polyakov, Phys. Rev. Lett. **95**, 206603 (2005).
[25] E. Altman and R. Vosk, Annu. Rev. Condens. Matter Phys. **6**, 383 (2015).
[26] Nandkishore and D. A. Huse, Annu. Rev. Condens. Matter Phys. **6**, 15 (2015).
[27] A. Abanin and Z. Papić, Ann. Phys. **529**, 1700169 (2017).
[28] N. Alet and N. Laflorencie, C. R. Phys. **19**, 498 (2018).
[29] D. A. Abanin, E. Altman, I. Bloch, and M. Serbyn, Rev. Mod. Phys. **91**, 021001 (2019).
[30] Ph. Jacquod and D. L. Shepelyansky, Phys. Rev. Lett. **79**, 1837 (1997).
[31] A. De Luca and A. Scardicchio, Europhys. Lett. **101**, 37003 (2013).
[32] S. Roy and D. E. Logan, Phys. Rev. B **101**, 134202 (2020).
[33] K. S. Tikhonov and A. D. Mirlin, Ann. Phys. **435**, 168525 (2021).
[34] L. Faoro, M. V. Feigel'man, and L. Ioffe, Ann. Phys. **409**, 167916 (2019).
[35] C. L. Baldwin and C. R. Laumann, Phys. Rev. B **97**, 224201 (2018).
[36] V. Smelyanskiy, K. Kechedzhi, S. Boixo, H. Neven, and B. Altshuler, arXiv:1907.01609.
[37] G. Biroli, D. Facoetti, M. Schiró, M. Tarzia, and P. Vivo, Phys. Rev. B **103**, 014204 (2021).
[38] T. Parolini and G. Mossi, arXiv:2007.00315.
[39] F. Wegner, Z. Phys. B **36**, 209 (1980).
[40] G. Biroli and M Tarzia, Phys. Rev. B **102**, 064211 (2020).
[41] K. S. Tikhonov and A. D. Mirlin, Phys. Rev. B **94**, 184203 (2016); M. Sonner, K. S. Tikhonov, and A. D. Mirlin, *ibid.* **96**, 214204 (2017).
[42] D. J. Luitz, N. Laflorencie, and F. Alet, Phys. Rev. B **93**, 060201(R) (2016).
[43] N. Macé, F. Alet, and N. Laflorencie, Phys. Rev. Lett. **123**, 180601 (2019).
[44] F. Pietracaprina and N. Laflorencie, Ann. Phys. **435**, 168502 (2021).
[45] G. De Tomasi, I. M. Khaymovich, F. Pollmann, and S. Warzel, Phys. Rev. B **104**, 024202 (2021).
[46] I. V. Gornyi, A. D. Mirlin, D. G. Polyakov, and A. L. Burin, Ann. der Phys. **529**, 1600360 (2017).
[47] K. S. Tikhonov and A. D. Mirlin, Phys. Rev. B **97**, 214205 (2018).
[48] M. Tarzia, Phys. Rev. B **102**, 014208 (2020).
[49] V. Ros, M. Müller, and A. Scardicchio, Nucl. Phys. B **891**, 420 (2015).
[50] M. Serbyn, Z. Papić, and D. A. Abanin, Phys. Rev. B **96**, 104201 (2017).

[51] D. J. Luitz, I. M. Khaymovich, and Y. Bar Lev, SciPost Phys. Core **2**, 006 (2020).

[52] V. E. Kravtsov, I. M. Khaymovich, E. Cuevas, and M. Amini, New J. Phys. **17**, 122002 (2015).

[53] V. E. Kravtsov, I. M. Khaymovich, B. L. Altshuler, and L. B. Ioffe, arXiv:2002.02979.

[54] I. M. Khaymovich, V. E. Kravtsov, B. L. Altshuler, and L. B. Ioffe, Phys. Rev. Research **2**, 043346 (2020).

[55] C. Monthus, J. Phys. A: Math. Theor. **50**, 295101 (2017).

[56] G. Biroli and M. Tarzia, Phys. Rev. B **103**, 104205 (2021).

[57] W. Buijsman and Y. Bar Lev, SciPost Phys. **12**, 082 (2022).

[58] I. M. Khaymovich and V. E. Kravtsov, SciPost Phys. **11**, 045 (2021).

[59] J. N. Bandyopadhyay, J. Wang, and J. Gong, Phys. Rev. E **81**, 066212 (2010).

[60] S. Ray, A. Ghosh, and S. Sinha, Phys. Rev. E **97**, 010101(R) (2018).

[61] M. Sarkar, R. Ghosh, A. Sen, and K. Sengupta, Phys. Rev. B **103**, 184309 (2021).

[62] S. Roy, I. M. Khaymovich, A. Das, and R. Moessner, SciPost Phys. **4**, 025 (2018).

[63] J. Wang, X.-J. Liu, G. Xianlong, and H. Hu, Phys. Rev. B **93**, 104504 (2016).

[64] P. A. Nosov, I. M. Khaymovich, and V. E. Kravtsov, Phys. Rev. B **99**, 104203 (2019).

[65] A. Duthie, S. Roy, and D. E. Logan, arXiv:2112.09856.

[66] A. G. Kutlin and I. M. Khaymovich, SciPost Phys. **11**, 101 (2021).

[67] V. Motamarri, A. S. Gorsky, and I. M. Khaymovich, arXiv:2112.05066.

[68] W. Tang and I. M. Khaymovich, arXiv:2112.09700.

[69] M. Pino, L. B. Ioffe, and B. L. Altshuler, Proc. Natl. Acad. Sci. USA **113**, 536 (2016); M. Pino, V. E. Kravtsov, B. L. Altshuler, and L. B. Ioffe, Phys. Rev. B **96**, 214205 (2017).

[70] K. Kechedzhi, V. N. Smelyanskiy, J. R. McClean, V. S. Denchev, M. Mohseni, S. V. Isakov, S. Boixo, B. L. Altshuler, and H. Neven, arXiv:1807.04792.

[71] T. Micklitz, F. Monteiro, and A. Altland, Phys. Rev. Lett. **123**, 125701 (2019); F. Monteiro, T. Micklitz, M. Tezuka, and A. Altland, Phys. Rev. Research **3**, 013023 (2021).

[72] P. von Soosten and S. Warzel, Lett. Math. Phys. **109**, 905 (2019).

[73] D. Facoetti, P. Vivo, and G. Biroli, Europhys. Lett. **115**, 47003 (2016).

[74] E. Bogomolny and M. Sieber, Phys. Rev. E **98**, 042116 (2018).

[75] G. de Tomasi, M. Amini, S. Bera, I. M. Khaymovich, and V. E. Kravtsov, SciPost Phys. **6**, 014 (2019).

[76] M. Pino, J. Tabanera, and P. Serna, J. Phys. A: Math. Theor. **52**, 475101 (2019).

[77] K. Truong and A. Ossipov, Europhys. Lett. **116**, 37002 (2016).

[78] M. Amini, Europhys. Lett. **117**, 30003 (2017).

[79] R. Berkovits, Phys. Rev. B **102**, 165140 (2020).

[80] R. Albert and A.-L. Barabási, Rev. Mod. Phys. **74**, 47 (2002).

[81] F. L. Metz and T. Peron, J. Phys.: Complexity (2022).

[82] L. Lovász, Random walks on graphs A survey, combinatorics, Paul Erdos is eighty. Bolyai Society. Mathematical Studies, 2(01) (1993).

[83] K. Broderix, T. Aspelmeier, A. K. Hartmann, and A. Zippelius, Phys. Rev. E **64**, 021404 (2001).

[84] A. Cavagna, I. Giardina, and G. Parisi, Phys. Rev. Lett. **83**, 108 (1999).

[85] F. L. Metz and J. D. Silva, Phys. Rev. Research **2**, 043116 (2020).

[86] B. Bollobás, *The Evolution of Random Graphs—The Giant Component*, Random Graphs Vol. 184 (Cambridge University Press, Cambridge, 2001).

[87] For $c = 1$ the number of vertices in the largest component of the graph is with high probability proportional to $N^{2/3}$.

[88] G. J. Rodgers and A. J. Bray, Phys. Rev. B **37**, 3557 (1988).

[89] A. J. Bray and G. J. Rodgers, Phys. Rev. B **38**, 11461 (1988).

[90] G. J. Rodgers, K. Austin, B. Kahng, and D. Kim, J. Phys. A: Math. Gen. **38**, 9431 (2005).

[91] Y. V. Fyodorov and A. D. Mirlin, J. Phys. A: Math. Gen. **24**, 2219 (1991).

[92] O. Khorunzhy, M. Shcherbina, and V. Vengerovsky, J. Math. Phys. **45**, 1648 (2004).

[93] R. Kühn, J. Phys. A: Math. Theor. **41**, 295002 (2008).

[94] G. Biroli and R. Monasson, J. Phys. A: Math. Gen. **32**, L255 (1999).

[95] G. Semerjian and L. F. Cugliandolo, J. Phys. A: Math. Gen. **35**, 4837 (2002).

[96] M. Mézard, G. Parisi, and M. Virasoro, *Spin Glass Theory and Beyond: An Introduction to the Replica Method and Its Applications* (World Scientific, Singapore, 1987).

[97] T. Rogers, I. Perez Castillo, R. Kühn, and K. Takeda, Phys. Rev. E **78**, 031116 (2008).

[98] V. A. R. Susca, P. Vivo, and R. Kühn, SciPost Phys. Lect. Notes **33** (2021).

[99] F. Benaych-Georges, C. Bordenave, and A. Knowles, Ann. Prob. **47**, 1653 (2019).

[100] F. Benaych-Georges, C. Bordenave, and A. Knowles, Ann. Inst. Henri Poincaré Probab. Stat. **56**, 2141 (2020).

[101] K. Tikhomirov and P. Youssef, Random Struct. Alg. **58**, 517 (2021).

[102] Note that this idea has also been exploited in the physics literature to characterize the Lifshitz tails of ER graphs when the average degree c is of order 1 in the context of the SDA [94,95].

[103] J. M. Combes and L. Thomas, Commun. Math. Phys. **34**, 251 (1973).

[104] F. Pietracaprina, V. Ros, and A. Scardicchio, Phys. Rev. B **93**, 054201 (2016).

[105] V. E. Kravtsov, B. L. Altshuler, and L. B. Ioffe, Ann. Phys. **389**, 148 (2018).

[106] C. Bordenave and M. Lelarge, Random Struct. Alg. **37**, 332 (2010).

[107] In practice, in order to estimate $N_{\rm loc}(\lambda)$, we solve Eq. (15) at fixed λ for several values of N, and plug the solution into the left hand side of Eq. (16) to check whether it is smaller or larger than 1. We then perform a linear fit of these values in the region in which they are close to 1. $N_{\rm loc}$ is then determined as the value of N at which the linear function that fits the data best crosses 1, and the error bars are estimated from the errors of such fit.

[108] V. Oganesyan and D. A. Huse, Phys. Rev. B **75**, 155111 (2007).

[109] Perhaps the best example of that is provided by the generalization of the Rosenzweig-Porter random matrix model of Ref. [52] (see also Ref. [56]), where there is a whole region

of the parameter space where wave functions are delocalized but multifractal and strongly correlated, while the statistics of neighboring gaps is still described by the GOE ensemble. In this case one numerically finds that $\langle q \rangle$ converges to its GOE universal value $2/\pi$ irrespective of the fact that wave functions amplitudes are not uncorrelated Gaussian random variables of variance $1/N$.

[110] E. Tarquini, G. Biroli, and M. Tarzia, Phys. Rev. Lett. **116**, 010601 (2016).

[111] G. Biroli, A. K. Hartmann, and M. Tarzia, Phys. Rev. B **105**, 094202 (2022)

[112] K. S. Tikhonov, A. D. Mirlin, and M. A. Skvortsov, Phys. Rev. B **94**, 220203(R) (2016).

[113] We have checked that computing the discrete logarithmic derivatives using 3 or 7 points does not modify significantly the results.

[114] I. Garcia-Mata, O. Giraud, B. Georgeot, J. Martin, R. Dubertrand, and G. Lemarié, Phys. Rev. Lett. **118**, 166801 (2017).

[115] B. L. Altshuler and B. I. Shklovskii, Zh. Eksp. Teor. Fiz. **91**, 220 (1986).

[116] J. T. Chalker, Physica A **167**, 253 (1990); J. T. Chalker and G. J. Daniell, Phys. Rev. Lett. **61**, 593 (1988).

[117] E. Cuevas and V. E. Kravtsov, Phys. Rev. B **76**, 235119 (2007).

[118] A. D. Mirlin, Phys. Rep. **326**, 259 (2000).

[119] B. Derrida, Phys. Rev. Lett. **45**, 79 (1980).

[120] C. R. Laumann, A. Pal, and A. Scardicchio, Phys. Rev. Lett. **113**, 200405 (2014).

[121] C. L. Baldwin, C. R. Laumann, A. Pal, and A. Scardicchio, Phys. Rev. B **93**, 024202 (2016).

[122] G. Biroli, A. C. Ribeiro-Teixeira, and M. Tarzia, arXiv:1211.7334.

[123] A. De Luca, B. L. Altshuler, V. E. Kravtsov, and A. Scardicchio, Phys. Rev. Lett. **113**, 046806 (2014); A. De Luca, A. Scardicchio, V. E. Kravtsov, and B. L. Altshuler, arXiv:1401.0019.

[124] B. L. Altshuler, E. Cuevas, L. B. Ioffe, and V. E. Kravtsov, Phys. Rev. Lett. **117**, 156601 (2016); B. L. Altshuler, L. B. Ioffe, and V. E. Kravtsov, arXiv:1610.00758.

[125] S. Bera, G. De Tomasi, I. M. Khaymovich, and A. Scardicchio, Phys. Rev. B **98**, 134205 (2018).

[126] G. De Tomasi, S. Bera, A. Scardicchio, and I. M. Khaymovich, Phys. Rev. B **101**, 100201(R) (2020).

[127] S. Savitz, C. Peng, and G. Refael, Phys. Rev. B **100**, 094201 (2019).

[128] M. Pino, Phys. Rev. Research **2**, 042031(R) (2020).

[129] F. L. Metz and I. P. Castillo, Phys. Rev. B **96**, 064202 (2017).